 CMES, vol.97, no.2, pp.131-174, 2014

Frequency Domain Based Solution for Certain Class of Wave Equations: An exhaustive study of Numerical Solutions

Vinita Chellappan[1], S. Gopalakrishnan[1] and V. Mani [1]

Abstract: The paper discusses the frequency domain based solution for a certain class of wave equations such as: a second order partial differential equation in one variable with constant and varying coefficients (Cantilever beam) and a coupled second order partial differential equation in two variables with constant and varying coefficients (Timoshenko beam). The exact solution of the Cantilever beam with uniform and varying cross-section and the Timoshenko beam with uniform cross-section is available. However, the exact solution for Timoshenko beam with varying cross-section is not available. Laplace spectral methods are used to solve these problems exactly in frequency domain. The numerical solution in frequency domain is done by discretisation in space by approximating the unknown function using spectral functions like Chebyshev polynomials, Legendre polynomials and also Normal polynomials. Different numerical methods such as Galerkin Method, Petrov- Galerkin method, Method of moments and Collocation method or the Pseudo-spectral method in frequency domain are studied and compared with the available exact solution. An approximate solution is also obtained for the Timoshenko beam with varying cross-section using Laplace Spectral Element Method (LSEM). The group speeds are computed exactly for the Cantilever beam and Timoshenko beam with uniform cross-section and is compared with the group speeds obtained numerically. The shear mode and the bending modes of the Timoshenko beam with uniform cross-section are separated numerically by applying a modulated pulse as the shear force and the corresponding group speeds for varying taper parameter m are obtained numerically by varying the frequency of the input pulse. An approximate expression for calculating group speeds corresponding to the shear mode and the bending mode, and also the cut-off frequency is obtained. Finally, we show that the cut-off frequency disappears for large m, for $\varepsilon > 0$ and increases for large m, for $\varepsilon < 0$.

Keywords: Partial differential equation, Spectral finite element method, Frequen-

[1] Department of Aerospace Engineering, Indian Institute of Science, Bangalore, India.

cy domain method, Timoshenko beam, group speed, cut-off frequency

1 Introduction

In this paper we discuss the numerical solution of partial differential equations (PDEs) using frequency domain approach for the following four classes of problems such as:
Problem (i) / Class (i): A cantilever beam of uniform cross-section.
Problem (ii) / Class (ii): A cantilever beam of varying cross-section.
Problem (iii) / Class (iii): A Timoshenko beam of uniform cross-section.
Problem (iv) / Class (iv): Timoshenko beam of varying cross-section.
Problem (i) is a second order PDE in one variable with constant coefficient, for which exact solution is available. Problem (ii) is a second order PDE in one variable with varying coefficients for which exact solution is available in the form of Bessel functions. The Timoshenko beam (Problem (iii)) is a second order coupled PDE with constant coefficients, for which exact solution is available. Problem ((iv)) is coupled second order PDE in two variables with varying coefficients. However, for Problem (iv) exact solution is not available. Problem (iii) and (iv) when decoupled leads to a fourth order PDE. We solve all the four problems using spectral methods. Numerical methods such as the Galerkin approach, Petrov-Galerkin approach, Method of Moments and the Pseudo-spectral approach in frequency domain are also formulated for all the above problems. The numerical methods in frequency domain are validated for problems for which exact solution is available (Problem (i), (ii) and (iii)). We then obtain solution to Problem (iv) numerically.

Various numerical methods are devised and are avialable in literature for the solution of PDEs of which the finite element methods, finite volume method, spectral method and Meshfree methods are quite popular. Solution of partial differential equations (PDE) in time domain using spectral function approximation in the spatial domain and then time marching in the temporal domain is quite popular [Boyd (2000),Cohen (2002)]. The time domain solution has been applied for solution of a class of Hamilton Jacobi Bellman equation called the Eikonal equation [Salehi and Dehghan (2012)], a generalised Kuramoto Sivashinsky (GKS) equation [Khater and Temsah (2008)], for a Heterogeneous Porous Media Flow [Black (1995)] etc., where different spectral methods are used for spatial discretisation.

An accuracy of finite element solutions for 3-D Timoshenko beams which is obtained using a co-rotational formulation is studied in [Iura, Suetake, and Atluri (2003)], where it is shown that the solutions converge to the exact beam theory as the number of elements increases. A number of numerical studies to deal with the 4^{th} order problem of thin beams like the meshless local Petrov Galerkin methods (MLPG) [Atluri, Cho, and Kim (1999)], where the beams under various loading

and boundary conditions are analysed and compared with the analytical solution. A 4^{th} order differential equation is used in [Atluri and Shen (2005)] to show that various mixed MLPG methods are cost effective. Also, MLPG methods are used in [Long and Atluri (2002)] for solving the bending problem of a thin plate using least square approximation to interpolate the solution variables.

The Chebyshev collocation method for solution of simple ordinary differential equations with examples is discussed in detail in [Saravi, Babolian, England, and Bromilow (2008)]. They have compared the results with the Adams method and has shown that the collocation method gives better rate of convergence compared to Adams method. In [Salehi and Dehghan (2012)], the Eikonal equation, which is a nonlinear partial differential equation for which exact solutions are usually difficult to obtain is numerically solved using Legendre pseudo-spectral viscosity techniques to discretise the problem in space. In [Khater and Temsah (2008)], the Chebyshev-spectral collocation method is used for spatial discretisation of the GKS equation. The spectral element technique in time domain, where the test function is different from the approximating polynomial is discussed in detail in [Black (1995)]. In this Petrov-Galerkin method is used for the spatial discretisation of a Heterogeneous Porous Media Flow and Adams-Bashforth/Crank Nicholson Scheme is used for temporal discretisation.

Here, in this paper we consider the spectral element method in frequency domain for the numerical solution of all the four problems.

Spectral methods using Fourier transforms for wave propagation analysis were popularised by [Doyle (1999)] and more recently by [Gopalakrishnan, Chakraborty, and Mahapatra (2006)]. Spectral finite element method (SFEM) is an effective tool used for solving wave propagation problems. It can be considered as a finite element method [Reddy (2005)] formulated in frequency domain. In SFEM, the governing partial differential equation is transformed in frequency domain using Discrete Fourier Transform (DFT) and is reduced to a set of ordinary differential equations (ODEs) with constant coefficients, with frequency as a parameter. The resulting ODE can be solved either analytically or numerically using spectral function approximation. Usually an exact solution to the governing ODEs in frequency domain is possible. In the absence of discontinuity, one single element is sufficient to handle a rod of any length. Spectral element for elementary rod [Doyle (1999)], elementary beam [Doyle and Farris (1990a,b)], Timoshenko beam [Gopalakrishnan, Martin, and Doyle (1992)], for elementary composite beam [Mahapatra and Gopalakrishnan (2003)], for functionally graded beams [Chakraborty and Gopalakrishnan (2003)] are reported in literature. In [Godinho and Soares Jr. (2013)] an optimised frequency domain iterative coupling algorithm is presented to analyze interacting acoustic elastodynamic models, which are discretized by sev-

eral different numerical methods discussed above. To avoid ill posed problems arising due to frequency domain wave propagation analyses an optimal iterative procedure for solid-fluid interactions is given in [Godinho and Soares Jr. (2012)].

In our recent study [Vinita, Gopalakrishnan, and Mani (2013)], the time domain analysis for solution of the wave equation for a uniform cross-section Cantilever beam is presented. In this study, the issues and challenges that arise in solving the wave equation in time domain and frequency domain is addressed. In our earlier study we have used both Lagrangian and Hermite interpolation for representation in spatial domain. In this paper, we use the Lagrangian interpolation for representation of the unknown function.

We discuss the performance of the four class of problems by considering:

(1) *Effect of the number of FFT points used (N_s)*

(2) *Effect of the order of the polynomial (N) used for approximation*

(3) *Effect of the number of segments (elements) (S) used*

(4) *Effect of frequency (f) on the group speeds (c_g)*

(5) *Observation of the shear mode and the bending mode for the Timoshenko beam by using a modulated pulse*

(6) *Effect of the taper parameter m on the group speeds (c_g) for Problem (ii) and Problem (iv)*

(7) *Computation of group speeds for the Timoshenko beam with varying coefficient for which an analytical expression is not available*

We can use the Fourier spectral analysis for all the four problems. But this introduces signal wrap around effects. One way of avoiding wrap around effect is by increasing the time window T, or by providing an artificial damping to the system. Another way of avoiding wrap around effect is by using a throw off element which makes the transfer function complex, thereby providing sufficient damping to the system. Also, wrap around effects do not exist if one uses Wavelet transforms and Laplace transforms. The wavelet transform based finite element analysis for composite beams are discussed in [Mitra and Gopalakrishnan (2006)]. The wavelet transform does not suffer from wrap around problems since the periodicity assumption is not used in constructing the transform, but lacks frequency resolution. It is shown that the wrap around effects are reduced as a result of taking the Laplace Transform of the unknown axial displacement in place of Fourier transform [Murthy, Gopalakrishnan, and Nair (2011)]. Hence in our study, we have used the Laplace transform method for solution of the all the four problems. We also use Laplace spectral element method (LSEM) for an approximate solution to Problem (iv).

For approximate solution in frequency domain analysis, the set of ODEs in frequency domain is solved numerically using variational principles, by approximating in spatial domain using spectral functions like Chebyshev and Legendre polynomials. The method of weighted residuals [Reddy (2005)] is used for an approximate solution in the spatial domain. We also study the various numerical methods like Galerkin approach, Petrov-Galerkin approach, Method of Moments approach and the Collocation approach [Boyd (2000); Canuto, Quarteroni, Hussaini, and Zang (2006)]. We compare all the numerical methods with the exact solution available for Problem (i), (ii) and (iii). For the Timoshenko beam with variable coefficients (Problem (iv)), we present the numerical solution.

We also obtain the group speed for varying taper parameter m, by varying the frequency of the input pulse. We then show that the modulated pulse is able to extract the shear mode and the bending mode of the Timoshenko beam. We also observe the effect of taper parameter m on the shear mode for fixed ε for Problem (iv).

It is also shown that the group speeds of the shear mode and the bending modes vary with frequency and taper parameter m for the Timoshenko beam with varying coefficients (Problem (iv)). Since the computation of the group speeds is not possible analytically for the Timoshenko beam with varying cross-section, we use the numerical methods to compute the group speeds. We form an approximate expression for the computation of the group speed and the cut-off frequency for Problem (iv)), Finally, we show that the cut-off frequency disappears for large m for $\varepsilon > 0$ and increases for large m for $\varepsilon < 0$.

2 Problem description

We define all the four problems in detail.

2.1 Problem(i)*: Cantilever beam of uniform cross-section*

The governing partial differential equation for the axial displacement ($u(x,t)$), in space and time of an undamped rod with uniform cross-section A_0 (Fig. 1.a)), in a given domain defined by the wave equation, is a second order partial differential equation in one variable is given as,

$$EA_0\frac{\partial^2 u}{\partial x^2}(x,t) - \rho A_0\frac{\partial^2 u}{\partial t^2}(x,t) = 0, \quad 0 < x < L \tag{1}$$

with boundary conditions, $u(0,t) = 0$ and $EA_0\frac{\partial u}{\partial x}(L,t) = F_L$.

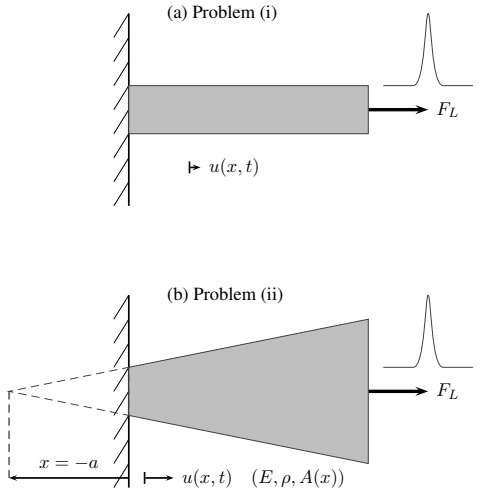

Figure 1: Cantilever beam

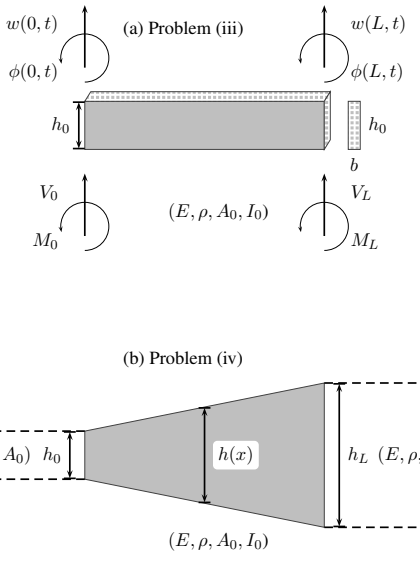

Figure 2: Timoshenko beam

2.2 Problem (ii): *Cantilever beam of varying cross-section*

The governing partial differential equation for the axial displacement ($u(x,t)$), in space and time of an undamped rod with varying cross-section $A(x)$, in a given domain defined by the wave equation, is a second order partial differential equation in one variable with varying coefficients as,

$$\frac{\partial}{\partial x}\left(EA(x)\frac{\partial u}{\partial x}(x,t)\right)-\rho A(x)\frac{\partial^2 u}{\partial t^2}(x,t)=0, \quad 0<x<L \tag{2}$$

with boundary conditions, $u(0,t)=0$ and $EA(L)\frac{\partial u}{\partial x}(L,t)=F_L$. Here, the area of cross-section is assumed to vary in the form as in [Doyle (1999)], with $A(x)=A_0\left(\frac{a+x}{a}\right)^m$, where a is as shown in (Fig. 1.b) and m is the taper. This above form leads to an exact solution in the form of Bessel functions in frequency domain. For Problem (i) and Problem (ii), we consider a cantilever beam of length L, Young's Modulus, E and density ρ. It is fixed at one end and is subjected to an axial force, F_L at the free (other) end, as shown in (Fig. 1). The axial displacement is $u(x,t)$ at a particular time. The initial conditions assumed for Problem (i) and Problem (ii) are, $u(x,0)=0$ and $\frac{\partial u}{\partial t}(x,0)=0$.

2.3 Problem (iii): *Timoshenko beam of uniform cross-section*

The Timoshenko beam is different from the Bernoulli beam as it also considers the shear deflection. The details of the derivation for the Timoshenko beam is given in [Doyle (1999); Reddy (2005)].

A Timoshenko beam of uniform cross-section is shown in (Fig. 2.a). The height of the beam at $x=0$ is $h(x)|_{x=0}=h_0$. The height $h(x)$ is uniform throughout the length of the beam, with $h(x)=h_0$, $x\in[0,L]$. Thus, the area of cross-section and the moment of inertia is a function of x and can be written as,

$$\begin{aligned} A(x) &= bh(x)=bh_0=A_0 \\ I(x) &= \frac{1}{12}bh^3(x)=\frac{1}{12}bh_0=I_0 \end{aligned} \tag{3}$$

The Timoshenko beam leads to two partial differential equations in two variables given as,

$$\frac{\partial}{\partial x}\left(GA(x)K\left(\frac{\partial w}{\partial x}-\phi\right)\right)=\rho A(x)\frac{\partial^2 w}{\partial t^2} \tag{4}$$

$$\frac{\partial}{\partial x}\left(EI(x)\frac{\partial \phi}{\partial x}\right)+GA(x)K\left(\frac{\partial w}{\partial x}-\phi\right)=\rho I(x)\frac{\partial^2 \phi}{\partial t^2} \tag{5}$$

Here, $w(x,t)$ is the transverse deflection and $\phi(x,t)$ is the shear deflection. Also, for uniform cross-section and constant coefficients, $A(x) = A_0$ and $I(x) = I_0$. The boundary conditions specified with $A(L) = A_0$ and $I(L) = I_0$ are,

$$\text{At } x = 0,\ w(0,t) = 0,\ \phi(0,t) = 0 \tag{6}$$

$$\text{At } x = L,\ GA(L)K\left(\frac{\partial w}{\partial x}(L,t) - \phi(L,t)\right) = V_L \text{ or } EI(L)\frac{\partial \phi}{\partial x}(L,t) = M_L \tag{7}$$

2.4 Problem(iv)*: Timoshenko beam of varying cross-section*

Here we consider a Timoshenko beam of varying height, with $h(x)|_{x=0} = h_0$. The height $h(x)$ varies along the length of the beam as $h(x) = h_0\left(1 + \frac{\varepsilon x}{L}\right)^m$, where $\varepsilon > 0$ and m specifies the taper. Thus, the area of cross-section and the moment of inertia can be written as a function of x as,

$$\begin{aligned} A(x) &= bh(x) = bh_0(1 + \frac{\varepsilon x}{L})^m = A_0(1 + \frac{\varepsilon x}{L})^m \\ I(x) &= \frac{1}{12}bh^3(x) = \frac{1}{12}bh_0(1 + \frac{\varepsilon x}{L})^m = I_0(1 + \frac{\varepsilon x}{L})^{3m} \end{aligned} \tag{8}$$

The partial differential equations in two variables for the Timoshenko beam with varying coefficients are the same as given by (Eq. 4) and (Eq. 5). The boundary conditions for the Timoshenko beam of varying cross-section are given by (Eq. 6) and (Eq. 7).

The initial conditions assumed for Problem (iii) and (iv) of Timoshenko beam are $w(x,0) = 0$, $\frac{\partial w}{\partial t}(x,0) = 0$, and $\phi(x,0) = 0$, $\frac{\partial \phi}{\partial t}(x,0) = 0$. For Problem (iii) and (iv), we consider a Timoshenko beam of length L and constant width b, with Young's Modulus E, density ρ and shear modulus $G = \frac{1}{2(1+\nu)}$. Here ν is the Poisson's ratio. The boundary conditions at $x = L$, is either specified as a shear force V_L or a Moment force M_L as defined by (Eq. 7).

For all the four problems, the axial force, F_L in Problem (i) and (ii), the shear force V_L and Moment force M_L in (Eq. 7) is taken either to be a Gaussian pulse or a modulated pulse given by:

$$\text{Gaussian pulse, } F_L/V_L/M_L = \frac{1}{\sqrt{2\pi\sigma^2}}e^{-\frac{(t-\mu)^2}{2\sigma^2}} \tag{9}$$

$$\text{Modulated pulse, } F_L/V_L/M_L = \sin(2\pi f t).\cos(\frac{1}{T_{pulse}}t) \tag{10}$$

Here, μ is the mean and σ^2 is the variance. The pulse width is essentially controlled by the variance parameter σ for the Gaussian pulse. For the modulated pulse, f is the frequency and T_{pulse} is the time period of the pulse.

The forcing function ($F_L/V_L/M_L$), in the form of a Gaussian pulse and a modulated pulse is shown in (Fig. 3) and (Fig. 4).

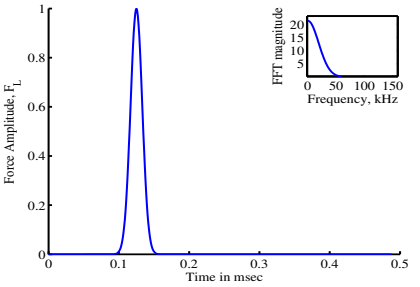

Figure 3: Forcing function, F_L is a Gaussian pulse applied at the free end of the rod

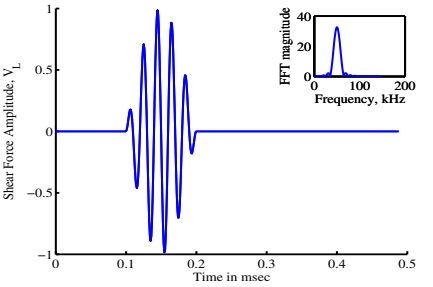

Figure 4: Forcing function, V_L is a modulated pulse applied at the free end of the rod

In the next section we present the exact solution of the cantilever beam and the Timoshenko beam in frequency domain.

3 Exact Solution in Frequency Domain

In this section, we first seek the exact solution for Problems (i), (ii) and (iii) in frequency domain using spectral analysis. For Problem (i), the solution of (Eq. 1) in time domain is well known and it is in the form of D'Alembert's solution, $u(x,t) = f(x-ct)+g(x+ct)$, where c is the velocity of the medium, given by $c = \sqrt{\frac{E}{\rho}}$. The functions f and g signify the incident and reflected waves respectively. However, obtaining the function f and g are not straight forward for all boundary conditions. For Problem (ii), the exact solution of (Eq. 2) for the cantilever beam of varying cross-section is in the form of Bessel functions, where the area of cross-section varies in the form as given in section (2.2).

For Problem (iii) the exact solution for (Eq. 4) and (Eq. 5) is available in frequency domain. The difference between the rod and the beam is that the beam does not have a D' Alembert's solution and the solution itself is dispersive [Doyle (1999)]. Here we also consider a throw-off element attached at both the ends of the Timoshenko beam and we separate the shear mode and the bending mode. For Problem (iv), the exact solution for (Eq. 4) and (Eq. 5) is not available. We get the solution numerically and separate the shear mode and the bending mode for varying taper parameter m and ε.

Spectral methods using Fourier analysis have become very popular recently in wave propagation analysis. This is because, the Fourier transformation reduces the governing PDE into a set of ODEs and an analytical solution is possible for most of the 1-D waveguides. Spectral analysis using Fourier methods was first popularised in [Doyle (1999)] and a complete state of the art of spectral analysis is discussed in [Gopalakrishnan, Chakraborty, and Mahapatra (2006)]. Finite element method formulated in the frequency domain is known as the Spectral Finite Element Method (SFEM). Fourier based spectral finite element method (FSEM) has become a very efficient tool for solving wave propagation problems, due to its ability to handle problems involving high frequency signals. Usually, in FSEM one element is sufficient to handle structures without discontinuities. Fourier analysis is prone to signal processing errors due to periodicity assumption of signals both in time and frequency domain. A detailed description of the Fourier analysis for the cantilever beam was done as an initial study and is given in [Vinita, Gopalakrishnan, and Mani (2013)].

In [Vinita, Gopalakrishnan, and Mani (2013)] we have considered a throw off element to avoid signal wrap around effects. If we allow some leakage of the signal response from the fixed boundary, it introduces an artificial damping so that good resolution in the time response signal is obtained. The leakage is modelled using an infinite element at the fixed end of the rod; also called a throw off element [Doyle (1999); Gopalakrishnan, Chakraborty, and Mahapatra (2006)]. This makes the transfer function of the system in Problem (i) complex, indicating that the wave also attenuates as it propagates. That is, if the time window is large enough, the wraparound problems can be avoided. Problem (iii) is also modelled using a throw-off element attached at both the ends of the Timoshenko beam in order to avoid signal wrap around effects. Thus for an exact solution, we can also use the Fourier transform approach for the Timoshenko beam.

Another way of avoiding wrap around is by adding sufficient damping to the system by taking the Laplace transform of the signal instead of Fourier transform [Murthy, Gopalakrishnan, and Nair (2011)]. It is well known [Lathi (1998)] that the Laplace Transform can be seen as the Fourier Transform of an exponentially windowed signal. So in this paper, we discuss only the Laplace transform approach for a solution in frequency domain.

3.1 Problem (i) *: Cantilever beam of uniform cross-section*

For the exact solution we first take the Laplace transform of the unknown function, the axial displacement ($u(x,t)$), as $\hat{u}_n(x,s_n)$ and differentiate in space and time [Vinita, Gopalakrishnan, and Mani (2013)] and substitute the derivatives in the

governing (Eq. 1),

$$EA_0 \frac{d^2\hat{u}_n(x,s_n)}{dx^2} - \rho A_0 s_n^2 \hat{u}(x,s_n) = 0 \tag{11}$$

$$\frac{d^2\hat{u}_n(x,s_n)}{dx^2} + {k_n}^2 \hat{u}_n(x,s_n) = 0,\ n = 0,1,...,N_s-1 \tag{12}$$

where, k_n is the wavenumber defined as $k_n = -j\left(\sqrt{\frac{\rho A_0}{EA_0}}\right)s_n$. Here $s_n = \sigma + j\omega_n, \quad n = 0,1,...,N_s-1$, where σ is a positive real constant (the damping factor) which provides sufficient damping and ω_n is the angular frequency in radians. The value of σ is selected as, given in [Murthy, Gopalakrishnan, and Nair (2011)], by two different approximations, namely Wilcox and Wedepohl approximations. The corresponding boundary conditions are, $\hat{u}_n(0,s_n) = 0$ and $EA_0\frac{d\hat{u}_n(L,s_n)}{dx} = \hat{F}_L(s_n)$, for $n = 0,1,...,N_s-1$, where, $\hat{F}_L$ is Laplace transform of the forcing function, F_L. Thus, we have N_s second order homogeneous linear ordinary differential equations, which can be solved either analytically or using numerical methods. We attempt to obtain the solution exactly, $\hat{u}_n(x,s_n)$ in frequency domain. The exact solution for axial displacement, $\hat{u}_n(x,s_n)$ to the set of linear homogeneous second order ordinary differential (Eq. 12) is given by,

$$\hat{u}_n(x,s_n) = A_n e^{-jk_n x} + B_n e^{-jk_n(L-x)}, \qquad n = 0,1,...,N_s-1 \tag{13}$$

where, A_n and B_n are the incident and the reflected wave coefficients which needs to be determined using any of the two boundary conditions at the two ends of the rod, namely $x = 0$ and $x = L$. We need to solve for the coefficients A_n and B_n for only $n = 1,2,...,\frac{N_s}{2}$, since $u(x,t)$ is a real function [Doyle (1999)]. Once A_n and B_n are known, the axial displacement in frequency domain, $\hat{u}_n(x,s_n)$ can be obtained using (Eq. 13). The solution for axial displacement in time domain $u(x,t)$, is then obtained by taking the inverse Laplace transform.

3.2 **Problem (ii):** ***Cantilever beam of varying cross-section***

For a cantilever beam with varying cross-section, we substitute the derivatives of the axial displacement in the governing (Eq. 2), as,

$$E\frac{d}{dx}\left(A(x)\frac{d\hat{u}_n(x,s_n)}{dx}\right) - \rho A(x) s_n^2 \hat{u}(x,s_n) = 0 \tag{14}$$

$$(a+x)^2\frac{d^2\hat{u}(x,s_n)}{dx^2} + m(a+x)\frac{d\hat{u}(x,s_n)}{dx} + k_n^2(a+x)^2\hat{u}(x,s_n) = 0 \tag{15}$$

where, k_n is the wavenumber defined as $k_n = -j\left(\sqrt{\frac{\rho A_0}{EA_0}}\right)s_n$. (Eq. 15) is in the form of the generalised Bessel equation [Doyle (1999)] defined as,

$$z^2\frac{d^2\hat{u}}{dx^2} + (1+2\alpha)z\frac{d\hat{u}}{dx} + (\beta^2 z^{2\gamma} + \delta^2)\hat{u} = 0 \tag{16}$$

whose solution is given by, $\hat{u}_n = \frac{1}{z^\alpha}\left[A_n J_\nu(\frac{\beta z^\gamma}{\gamma}) + B_n Y_\nu(\frac{\beta z^\gamma}{\gamma})\right]$, where, J_ν and Y_ν are Bessel functions [Doyle (1999)] of the first and second kind respectively. The parameters defined in the Bessel (Eq. 16) are, $z = (a+x), \quad \beta = k_n, \gamma = 1, \delta = 0,$ and $\alpha = \frac{1}{2}(q-1)$. The corresponding boundary conditions are, $\hat{u}_n(0,s_n) = 0$ and $EA(L)\frac{d\hat{u}_n(L,s_n)}{dx} = \hat{F}_L(s_n)$, for $n = 0,1,...,N_s-1$, where, $\hat{F}_L$ is Laplace transform of the forcing function, $F_L(t)$. We now solve for the Bessel solution subjected to the boundary conditions. The results are obtained for different values of taper parameter m and a.

3.3 Problem (iii) *: Timoshenko beam of uniform cross-section*

For an exact solution, for the problem (iii), we first take the Laplace transform of the unknown function $w(x,t)$ and $\phi(x,t)$ as $\hat{w}_n(x,s_n)$ and $\hat{\phi}_n(x,s_n)$ as given in [Vinita, Gopalakrishnan, and Mani (2013)]. The Laplace transform of the (Eq. 4) and (Eq. 5), leads to two sets of (N_s) ordinary differential equations in two variables with constant coefficient given by,

$$\frac{d}{dx}\left(GA(x)K\left(\frac{d\hat{w}_n(x,s_n)}{dx} - \hat{\phi}_n(x,s_n)\right)\right) = \rho A(x)s_n^2\hat{w}_n(x,s_n) \tag{17}$$

$$\frac{d}{dx}\left(EI(x)\frac{d\hat{\phi}_n(x,s_n)}{dx}\right) + GA(x)K\left(\frac{d\hat{w}_n(x,s_n)}{dx} - \hat{\phi}_n(x,s_n)\right) = \rho I(x)s_n^2\hat{\phi}_n(x,s_n) \tag{18}$$

with $A(x) = A_0$ and $I(x) = I_0$, and boundary conditions,

$$\text{At } x = 0, \ \hat{w}_n(0,s_n) = 0, \ \hat{\phi}_n(0,s_n) = 0 \tag{19}$$

$$\text{At } x = L, \ GA_0K\left(\frac{d\hat{w}_n}{dx}(L,s_n) - \phi(L,s_n)\right) = V_L \text{ or } EI_0\frac{d\hat{\phi}_n}{dx}(L,s_n) = M_L \tag{20}$$

Let us assume a solution for the horizontal and shear deflection in frequency domain in the form, $\hat{w}_n(x,s_n) = \hat{w}_{n0}e^{-jk_nx}$, and $\hat{\phi}_n(x,s_n) = \hat{\phi}_{n0}e^{-jk_nx}$. Thus,

$$\begin{bmatrix} -GA_0Kk_n^2 - s_n^2\rho A_0 & jGA_0Kk_n \\ -jGA_0Kk_n & -EI_0k_n^2 - GA_0K - s_n^2\rho I_0 \end{bmatrix}\begin{bmatrix}\hat{w}_{n0}\\ \hat{\phi}_{n0}\end{bmatrix} = \begin{bmatrix}0\\0\end{bmatrix} \tag{21}$$

$$H(k_n)\begin{bmatrix}\hat{w}_{n0}\\ \hat{\phi}_{n0}\end{bmatrix}=\begin{bmatrix}0\\0\end{bmatrix} \tag{22}$$

The above (Eq. 22) has a non trivial solution only if $|H(k_n)|=0$, which is given by the characteristic equation as,

$$GA_0KEI_0k_n^4+\left(GA_0K\rho Is^2+\rho A_0EI_0s^2\right)k_n^2+\left(\rho I_0s^2+GA_0K\right)\rho As^2=0 \tag{23}$$

$$k_n^4+(k_{bn}^2+k_{sn}^2)k_n^2+(k_{bn}^2k_{sn}^2+k_{cn}^2)=0 \tag{24}$$

The coupling is not neglected here and we define, $k_{bn}=-j\sqrt{\frac{\rho I_0}{EI_0}}s_n, k_{sn}=-j\sqrt{\frac{\rho A_0}{GAK_0}}s_n$, and $k_{cn}=-j\sqrt{\frac{\rho A_0}{EI_0}}s_n$. Here k_{bn}, k_{sn} and k_{cn} can be called as the wave numbers corresponding to the different modes such bending, shear and also the coupling respectively. Finally, the wavenumber for the Timoshenko beam is given as,

$$k_n^2=k_{n1}^2,k_{n2}^2=\frac{-(k_{bn}^2+k_{sn}^2)\pm\sqrt{(k_{bn}^2+k_{sn}^2)^2-4(k_{bn}^2k_{sn}^2+k_{cn}^2)}}{2} \tag{25}$$

Thus the exact solution for the ODEs defined by (Eq. 17) and (Eq. 18) for an uniform Timoshenko beam is given as,

$$\hat{w}_n(x,s) = A_ne^{-jk_{n1}x}+B_ne^{-jk_{n1}(L-x)}+C_ne^{-jk_{n2}x}+D_ne^{-jk_{n2}(L-x)} \tag{26}$$

$$\begin{aligned}\hat{\phi}_n(x,s) &= \alpha_{n1}(k_{n1})A_ne^{-jk_{n1}x}-\alpha_{n1}(k_{n1})B_ne^{-jk_{n1}(L-x)}\ldots\\ &\quad \ldots+\alpha_{n2}(k_{n2})C_ne^{-jk_{n2}x}-\alpha_{n2}(k_{n2})D_ne^{-jk_{n2}(L-x)}\end{aligned} \tag{27}$$

Here α gives the relation between the horizontal deflection and shear deflection which can be derived from (Eq. 17) as, $\alpha_{ni}(k_{ni})=k_{ni}-\frac{k_{sn}^2}{k_{ni}}, \quad i=1,2$. The boundary conditions given in (Eq. 19) and (Eq. 20) are substituted in (Eq. 26) and (Eq. 27) to obtain $\hat{w}_n(x,s_n)$ and $\hat{\phi}_n(x,s_n)$. The horizontal deflection $w(x,t)$ and the shear deflection $\phi(x,t)$ in time domain is then obtained by inverse Laplace transform.

3.3.1 Throw off element:

We now consider a throw off element attached to both the ends of the Timoshenko beam. The use of throw off element for a uniform rod is discussed in [Vinita, Gopalakrishnan, and Mani (2013)]. We obtain the shear and bending modes separately for the Timoshenko beam without reflections from the boundary for the exact case. The throw off element attached at the boundary of the Timoshenko beam is formulated by neglecting the reflected coefficients B_n and D_n in (Eq. 26) and (Eq. 27).

For the infinite segment we assume an uniform cross-sectional area, A_∞ and moment of inertia, I_∞ equivalent to that at the boundaries ($x = 0$ and $x = L$) of the beam. A throw off element attached at the boundary of a varying cross-section Timoshenko beam is shown in (Fig. 2.b). Thus, the solution for the horizontal and shear deflection for the Timoshenko beam at infinite segments on either ends is given by,

$$\hat{w}_{l\infty_n}(x,s_n) = A_{l\infty_n}e^{-jk_{n1}x} + C_{l\infty_n}e^{-jk_{n2}x} \tag{28}$$

$$\hat{\phi}_{l\infty_n}(x,s_n) = \alpha_{n1}(k_{n1})A_{l\infty_n}e^{-jk_{n1}x} + \alpha_{n2}(k_{n2})C_{l\infty_n}e^{-jk_{n2}x} \tag{29}$$

$$\hat{w}_{r\infty_n}(x,s_n) = A_{r\infty_n}e^{-jk_{n1}x} + C_{r\infty_n}e^{-jk_{n2}x} \tag{30}$$

$$\hat{\phi}_{r\infty_n}(x,s_n) = \alpha_{n1}(k_{n1})A_{r\infty_n}e^{-jk_{n1}x} + \alpha_{n2}(k_{n2})C_{r\infty_n}e^{-jk_{n2}x} \tag{31}$$

Here the subscripts l and r stands for infinite segments attached at the left and right of the Timoshenko beam. The solution for the finite segment of Timoshenko beam is as given by (Eq. 26) and (Eq. 27). At the interface between the infinite and the finite waveguide, we have the following boundary conditions. That is, at $x = 0$, we have, $\hat{w}_{l\infty_n}(0,s_n) = \hat{w}_n(0,s_n), \hat{\phi}_{l\infty_n}(x,s_n) = \hat{\phi}_n(0,s_n)$ and $G_{l\infty}A_{l\infty}K\frac{\partial \hat{w}_{l\infty_n}}{\partial x}(0,s_n) = GA_0\frac{\partial \hat{w}_n}{\partial x}(0,s_n), E_{l\infty}I_{l\infty}\frac{\partial \hat{\phi}_{l\infty_n}}{\partial x}(0,s_n) = EI_0\frac{\partial \hat{\phi}_n}{\partial x}(0,s_n)$. At $x = L$, we have, $\hat{w}_{r\infty_n}(0,s_n) = \hat{w}_n(L,s_n), \hat{\phi}_{r\infty_n}(0,s_n) = \hat{\phi}_n(0,s_n)$ and $G_{r\infty}A_{r\infty}K\frac{\partial \hat{w}_{r\infty_n}}{\partial x}(L,s_n) + GA_0\frac{\partial \hat{w}_n}{\partial x}(L,s_n) = \hat{V}_L$, $E_{r\infty}I_{r\infty}\frac{\partial \hat{\phi}_{r\infty_n}}{\partial x}(L,s_n) + EI_0\frac{\partial \hat{\phi}_n}{\partial x}(L,s_n) = \hat{M}_L$. Now, imposing the above boundary conditions on (Eq. 28) to (Eq. 31) and (Eq. 26) and (Eq. 27) , we obtain $\hat{w}_n(x,s_n)$ and $\hat{\phi}_n(x,s_n)$. The horizontal deflection $w(x,t)$ and the shear deflection $\phi(x,t)$ in time domain is obtained by inverse Laplace transform.

Note that for Problem (iii), the modeling using throw off element aids in formulation also using the Fourier transform approach. This is because use of a throw off element avoids signal wrap around problems, as there is no reflection from the boundaries.

3.4 Problem (iv): *Timoshenko beam of varying cross-section*

Timoshenko beam of varying cross-section does not have an exact solution. Here, we use numerical methods for the solution. We discuss the numerical solution using spectral functions such as Chebyshev polynomials, Legendre polynomials and the Normal polynomials later in the paper. We try the different numerical methods such as the Galerkin approach, Petrov-Galerkin approach, Method of Moments and the Pseudo-spectral/Collocation Method for a solution.

4 Derivation of the group speeds, phase speed and the corresponding time

In this section, we derive the phase speeds and the group speeds of the cantilever beam and the Timoshenko beam. We consider the case for the damping factor, $\sigma = 0$. We observe the phase speeds and group speeds using numerical computation and validate the results with the exact solution for the cantilever beam and the Timoshenko beam. This helps in observing the speeds for cases where exact solution is not available (Problem (iv)). The phase speed and the group speed is defined as [Doyle (1999)], as $c_{ph} = \frac{\omega}{k_n}$ and $c_g = \frac{d\omega}{k_n}$ respectively.

4.1 Problem (i) and (ii): *Cantilever beam of uniform and varying cross-section*

The phase speed and group speeds are given as, $c_{ph} = \frac{\omega}{k_n} = \sqrt{\frac{E}{\rho}}$ and $c_g = \frac{d\omega}{k_n} = \sqrt{\frac{E}{\rho}}$ respectively. Note that the phase speeds and the group speeds are independent of the frequency $f_n = \frac{\omega_n}{2\pi}$, and area of cross-section and hence are the same.

4.2 Problem (iii): *Timoshenko beam of uniform cross-section*

The corresponding phase velocities and the group velocities for the Timoshenko beam can be obtained as, $c_{ph_{ni}} = \frac{\omega_n}{k_{ni}}$, and $c_{g_{ni}} = \frac{d\omega_n}{dk_{ni}}$, for $i = 1,2$ respectively. Hence the group speeds varies with the frequency as,

$$c_{g_{ni}} = \frac{2k_{ni}}{-(k_b^2 + k_s^2)\omega_n \pm \frac{2(k_b^2 - k_s^2)\omega_n^3 - 4k_c^2\omega_n}{2\sqrt{(k_{bn}^2 - k_{sn}^2) - 4k_c n^2}}} \quad i = 1,2 \tag{32}$$

where, $k_b = \sqrt{\frac{\rho I_0}{EI_0}}$, $k_s = \sqrt{\frac{\rho A_0}{GAK_0}}$, and $k_c = \sqrt{\frac{\rho A_0}{EI_0}}$. Also, for a particular frequency of the input pulse, the group speed $c_{g_{ni}}$ is used to calculate t (time required) as, $t = \frac{L}{c_{g_{ni}}}$, for $i = 1,2$. Here $i = 1,2$ represents the bending mode and the shear mode. We also obtain the group speeds for both the bending and shear mode numerically by varying the input frequency. The numerical results obtained for Problem (iii) is validated by the exact group speeds given by (Eq. 32). The results are discussed later.

4.3 Problem (iv): *Timoshenko beam of varying cross-section*

It is not possible to get the phase speeds and the group speeds exactly for the Timoshenko beam with varying area of cross-section. We get the group speeds numerically for varying taper parameter m, by varying the frequency of the input pulse. The variation of the group speeds with frequency is then plotted for both the shear mode and bending modes. The results are discussed later in the paper.

5 Numerical solution

In this paper, we analyse the performance of the numerical solution obtained using frequency domain analysis. For this, we first compare the numerical solution with the available exact solution for Problem (i), Problem (ii) and Problem (iii). For Problem (iv), as mentioned earlier, exact solution is not available, hence an approximate solution is obtained using the numerical methods.

5.0.1 Solution approach

The fundamental approach to most of the numerical methods is the weighted residual technique [Reddy (2005)] and is discussed in [Vinita, Gopalakrishnan, and Mani (2013)], where in the domain of interest is split up into many sub elements there by constructing a grid or mesh of the domain. Each mesh has a definite number of grid points or nodes and the variation of the dependent variable is expressed in terms of the values at the grid points that make up the single sub element. Such a relation is known as the shape function. For an approximate solution, we use classical variational method, which leads to the Method of Weighted Residuals [Reddy (2005); Boyd (2000)] where the residual is made zero in a weighted integral sense. In this paper we discuss the weak form of the weighted integral form of the governing differential equation to obtain the solutions.

For all the four Problems (i) to (iv), we can use either Fourier, or Laplace transform to transform the corresponding PDEs to ODEs in frequency domain. In our study, we use the Laplace transform. For Problem (i) and (ii), (Eq. 1) and (Eq. 2) in time domain is given by (Eq. 11) and (Eq. 14) for $n = 0, 1, ..., N_s - 1$ in the Laplace domain. Similarly, for Problem (iii) and (iv), (Eq. 4 and (Eq. 5) in time domain are given by (Eq. 17) and (Eq. 18) for $n = 0, 1, ..., N_s - 1$ in the Laplace domain.

The weighted residual technique and the weak form formulation reduces (Eq. 11) and (Eq. 14) and the the corresponding (Eq. 17) and (Eq. 18) to the form respectively as,

$$[K]\hat{u}_n + s^2[M]\hat{u}_n = \hat{f}_n \text{ and } [K_D]\begin{bmatrix}\hat{w}_n \\ \hat{\phi}_n\end{bmatrix} = \hat{f}_n, \tag{33}$$

where $[K]$ and $[M]$ are the stiffness and the mass matrix and $[K_D]$ is the dynamic stiffness matrix, $\hat{u}_n$, $\hat{w}_n$ and $\hat{\phi}_n$ are the corresponding response vectors in frequency domain. $\hat{f}_n$ is the force vector in frequency domain. This above equation is solved for $\hat{u}_n$, $\hat{w}_n$ and $\hat{\phi}_n$ for a given $\hat{f}_n$ and the response in time domain is obtained using the inverse Laplace transform.

Any numerical method including the weighted residual method in frequency domain require a grid (or elements). Over each grid (element), a set of solutions are

assumed, which are synthesised over all elements to obtain global solution. The nature of the solution assumed in Weighted Residual technique determine the type of numerical method, which in turn fixes the nodal points on the grid. For spatial discretisation in frequency domain, we consider $N+1$ interpolation points (or grid points/nodes), where N is the order of interpolating polynomial. The problem domain, $[x_0, x_f]$ is divided into N partitions of equal or variable length, with $N+1$ interpolation points (or grid points/nodes). Thus, the unknown function in frequency domain, can be approximated using an N^{th} order polynomial function in the interval $[x_0, x_f]$. The approximating function, approaches the exact solution in frequency domain as $N \to \infty$. The selection of the grid points and the polynomials for the approximation are briefly discussed in the next two sections.

5.1 Selection of Grid points or nodes

The grids are selected based upon quadrature rules. Quadrature rule depends on the type of method employed under Weighted Residual method to solve the problem. If we use the standard Galerkin procedure under Weighted Residual technique, we will normally use Gauss Quadrature rule to integrate to obtain the matrices $[K], [M]$ and $[K_D]$ in (Eq. 33). On the other hand if we choose orthogonal polynomials such as Chebyshev or Legendre polynomials as basis functions, then we will use Gauss Lobatto integration rule to obtain $[K]$, $[M]$ and $[K_D]$. The difference between the former and the latter integration is that in the latter, the integration points coincides with the nodal points, which will make $[M]$ in (Eq. 33) diagonal.

Thus, we can have Gauss, Gauss-Radau or Gauss Lobatto grids as given in [Canuto, Quarteroni, Hussaini, and Zang (2006)]. The advantage of the above grids over uniform grid is that they have the distribution property that, they cluster around the endpoints of the interval. The Gauss-Lobatto grid points are found to have the least error. The Chebyshev Gauss Lobatto points, (CGL) are extensively used in earlier studies [Canuto, Quarteroni, Hussaini, and Zang (2006)], as the interpolation at the CGL nodes gives the closest approximation to a given function. Also, CGL points result in the avoidance of the Runge phenomenon [Canuto, Quarteroni, Hussaini, and Zang (2006)]. Hence, CGL points are used in this paper.

The CGL points are the roots of the Chebyshev differential equation, and are given in closed form as, $x_n = -cos(\frac{n\pi}{N})$ for $n = 0, ..., N$. These points lying in the interval [-1,1] are the extrema of the N^{th} order Chebyshev polynomial $T_N(x)$, defined as $T_n(x) = cos(ncos^{-1}x)$. Our problem is specified in the interval $[x_0, x_f]$. Thus, for our problem, we have the shifted CGL points (or grid points) defined as, $x_i = \frac{(x_f - x_0)x_n + (x_0 + x_f)}{2}$ where, x_n are the nodes corresponding to the interval [-1,1]. For our problem, $x_0 = 0$ and $x_f = L$.

5.2 Selection of trial and test functions

In general, the axial displacement in frequency domain ($\hat{u}_n(x,s_n)$) of the Cantilever beam, the horizontal displacement ($\hat{w}_n(x,s_n)$) and the shear deflection ($\hat{\phi}_n(x,s_n)$) in frequency domain for the Timoshenko beam is approximated as a linear combination of the trial function ϕ_i, for $i = 1,2,..,N$ and the test function $v(x)$, is approximated as a weighted linear combination of functions ψ_i, for $i = 1,2,..,N$. The polynomials used as approximation functions are Chebyshev polynomials ($T_n(x)$), the Legendre polynomials ($P_n(x)$) and the Normal polynomials ($K_n(x)$). Depending upon the choice of the trial and the test functions, we have different numerical methods like the Galerkin method, Petrov-Galerkin method, Method of Moments and the Pseudospectral method. The different polynomials used and the different numerical methods are detailed in our technical report [Vinita, Gopalakrishnan, and Mani (2013)].

For the cantilever beam with uniform cross-section (Problem (i)) and with varying cross-section (Problem (ii)), we have only one dependent variable, the axial displacement ($u(x,t)$). For the weighted form for Problem (i) and (ii), we consider the test function with the same units as the axial displacement $v_u(x)$.

For the Timoshenko beam with uniform cross-section (Problem (iii)) and with varying cross-section (Problem (iv)), we have two dependent variables namely the horizontal deflection ($w(x,t)$) and the shear deflection ($\phi(x,t)$). Hence for Problem (iii) and (iv), we need to consider the test functions corresponding to the horizontal deflection $v_w(x)$ and also the test function corresponding to the shear deflection $v_\phi(x)$.

Lagrangian Interpolation and Shape functions: Here, for ease of computation, we use the Lagrangian interpolation, in which, the trial function (unknown function) $\hat{u}_n^N(x,s_n), \hat{w}_n^N(x,s_n), \hat{\phi}_n^N(x,s_n)$ and the test function $v(x)$ are represented as a function of function values at the grid points. Hermite interpolation can also be used for representation of the unknown function. The representation using the shape functions are described in detail in [Vinita, Gopalakrishnan, and Mani (2013)].

Problem (i) and (ii):*Representation of the axial displacement and the test function*

In general, the approximate solution in frequency domain ($\hat{u}_n^N(x,s_n)$), and the corresponding test function can be represented using any of the trial functions, ϕ_i (Chebyshev or Legendre or Normal polynomial) and finally we can represent the unknown function and the test function using the corresponding shape functions as,

$$\hat{u}_n^N(x,s_n) = \sum_{k=0}^{N} N_{uk}(x)\hat{u}_n^N(x_k,s_n), \quad v_u^N(x) = \sum_{k=0}^{N} N_{vk}(x)v^N(x_k) \tag{34}$$

Problem (iii) and (iv): *Representation of horizontal deflection, shear deflection*

and the test function

Similarly the unknown functions in the Timoshenko beam ($\hat{w}_n^N(x,s_n)$,$\hat{\phi}_n^N(x,s_n)$), and the corresponding test functions can be represented using any of the trial functions (Chebyshev or Legendre or Normal polynomial) and finally we can represent each unknown function and their corresponding test functions using the shape functions as,

$$\hat{w}_n^N(x,s_n) = \sum_{k=0}^{N} N_{wk}(x)\hat{w}_n^N(x_k,s_n), \quad \hat{\phi}_n^N(x,s_n) = \sum_{k=0}^{N} N_{\phi k}(x)\hat{\phi}_n^N(x_k,s_n) \tag{35}$$

$$v_w^N(x) = \sum_{k=0}^{N} N_{v_w k}(x){v_w}^N(x_k), \quad v_\phi^N(x) = \sum_{k=0}^{N} N_{v_\phi k}(x){v_\phi}^N(x_k) \tag{36}$$

Here $N_{(.)_k}$ is the shape function with $\sum_{k=0}^{N} N_{(.)k} = 1$. In the next section, we formulate the weak form of the weighted integral form of the differential equations for the cantilever beam and the Timoshenko beam. The formulations for each case is done separately.

6 Weak form formulation

We see that for the corresponding differential equations for the Cantilever beam and Timoshenko beam (Eq. 11), (Eq. 14), (Eq. 17) and (Eq. 18)), the differential operator $\mathscr{L}$ is of the order of 2. We expect that our solution be 2^{nd} order continuous or in other words $(u,w,\phi) \in C^2(0,L)$. Now the order of the differential of the unknown functions ($\frac{d^n u}{dx^n}$, $\frac{d^n w}{dx^n}$ and $\frac{d^n \phi}{dx^n}$) can be reduced if we distribute the differential of the unknown function to the weighting function, v_i in the weighted residual form. Thus, the weighted residual form reduces to the weak form of the corresponding differential equation. This can be achieved using integration by parts, of the weighted residual form of equation [Boyd (2000); Reddy (2005)] and the advantage of reducing the differential equation to the weak form is that it increases the solution space.

Thus, for a second order differential operator $\mathscr{L}$, we require that the function $(u,w,\phi) \in C^1(0,L)$. Thus, we have larger solution subspace to search for u,w and ϕ. Another advantage is that, the weak form of a self adjoint operator $\mathscr{L}$ leads to a symmetric matrix for $[K]$, $[M]$ and $[K_D]$ in (Eq. 33). Computation with symmetric matrices are more efficient as special algorithms are available. Moreover, the boundary conditions are directly embedded in the weak form formulation. The weak form formulation in frequency domain and time domain approach is discussed in the next section. The weak form formulation and the solution to the wave equation for the cantilever beam of uniform cross-section (Problem (i)) is given in

detail in our technical report [Vinita, Gopalakrishnan, and Mani (2013)]. The formulation of the varying case can also be obtained on similar lines. Hence in this section we consider only Problem (iii) and (iv).

6.1 Problem (iii) and (iv): *Weak form formulation and solution to the weak form*

In this section we consider the weak form formulation for the Timoshenko beam of varying cross-section (Problem (iv)). The formulation for the the uniform case (Problem (iii)) can be derived from the varying case by considering $A(x) = A_0, \forall x \in [0,L]$ and for the varying problem (Problem (iv)) $A(x) = A_0\left(1+\frac{\varepsilon x}{L}\right)^m, \forall x \in [0,L]$. Consider (Eq. 17) and (Eq. 18) for the Timoshenko beam of varying cross-section (Problem (iv)). The weighted integral form for the above referred differential equations is,

$$\int_0^L \left(\left(GA(x)K\left(\hat{w}_n' - \hat{\phi}_n\right)\right)' - s_n^2 \rho A(x)\hat{w}_n \right). \; v_w(x)dx = 0 \tag{37}$$

$$\int_0^L \left(\left(EI(x)\hat{\phi}_n'\right)' + GA(x)K\left(\hat{w}_n' - \hat{\phi}_n\right) - s_n^2 \rho I(x)\hat{\phi}_n \right). \; v_\phi(x)dx = 0, \quad n = 0,1,2,...,N_s-1 \tag{38}$$

In the above equation, $\hat{w}_n = \hat{w}_n(x,s_n)$ and $\hat{\phi}_n = \hat{\phi}_n(x,s_n)$ is the Laplace transform of $w(x,t)$ and $\phi(x,t)$ respectively and $v_w(x)$ and $v_\phi(x)$ are the test functions which have the same units as the horizontal deflection and the shear deflection respectively. Also, $(.)' = \frac{\partial(.)}{\partial x}$, $(.)'' = \frac{\partial^2(.)}{\partial x^2}$. Integrating the above (Eq. 37) and (Eq. 38), we can get the weak form of the corresponding equations. Now, the variational problem can be defined as, to find $\hat{w}_n(x,s_n)$ and $\hat{\phi}_n(x,s_n)$ such that the weak form of the wave equations are satisfied. Also, the boundary conditions are directly embedded in the weak form. We seek a solution for the weak form by approximating $\hat{w}_n(x,s_n), \hat{\phi}_n(x,s_n)$ and $v_w(x)$ and $v_\phi(x)$ as $\hat{w}_n^N(x,s_n), \hat{\phi}_n^N(x,s_n)$ and $v_w^N(x)$ and $v_\phi^N(x)$ and its corresponding derivatives in the weak form. We know that at the boundary $x = L$ and $x = 0$, $GA(L)K\left(\frac{d\hat{w}_n^N(L,s_n)}{dx} - \hat{\phi}_n^N(L,sn)\right) = \hat{V}_L$ and $N_{v_w i}(0)\ (GA(0)K\left(\frac{d\hat{w}_n^N(0,s_n)}{dx} - \hat{\phi}_n^N(0,sn)\right) = 0$. Applying these boundary conditions and substituting $\hat{w}_n^N(x,s_n)$ and $\hat{\phi}_n^N(x,s_n)$ and its derivatives in the weak form of the

Timoshenko beam for $n = 0, 1, 2..., N_s - 1$ we get,

$$N_{v_w i}(L)\hat{V}_L - GK\sum_{j=0}^{N}\int_0^L A(x)N'_{v_w i}N'_{w j}\hat{\mathbf{W}}_{\mathbf{nj}}dx + GK\sum_{j=0}^{N}\int_0^L A(x)N'_{v_w i}N_{\phi j}\hat{\Phi}_{nj}dx...$$
$$... - s_n^2\rho\sum_{j=0}^{N}\int_0^L A(x)N_{vi}N_{w j}\hat{\mathbf{W}}_{\mathbf{nj}}dx = 0 \tag{39}$$

$$N_{v_\phi i}(L)\hat{M}_L - E\sum_{j=0}^{N}\int_0^L I(x)N'_{v_\phi i}N'_{\phi j}\hat{\Phi}_{nj}dx + GK\sum_{j=0}^{N}\int_0^L A(x)N_{v_\phi i}N'_{w j}\hat{\mathbf{W}}_{\mathbf{nj}}dx...$$
$$... - GK\sum_{j=0}^{N}\int_0^L A(x)N_{v_\phi i}N_{\phi j}\hat{\Phi}_{nj}dx - s_n^2\rho\sum_{j=0}^{N}\int_0^L I(x)N_{v_\phi i}N_{\phi j}\hat{\Phi}_{nj}dx = 0 \tag{40}$$

Here $i = 0, 1, 2, ..., N$. The boundary conditions are specified either as shear force V_L or moment force M_L. Also, $\hat{\mathbf{W}}_\mathbf{n} = \begin{bmatrix}\hat{w}_n^N(x_0,s_n) & \hat{w}_n^N(x_1,s_n) & ... & \hat{w}_n^N(x_N,s_n)\end{bmatrix}^T$, and $\hat{\Phi}_n = \begin{bmatrix}\hat{\phi}_n^N(x_0,s_n) & \hat{\phi}_n^N(x_1,s_n) & ... & \hat{\phi}_n^N(x_N,s_n)\end{bmatrix}^T$ is the approximate solution to the weak form in frequency domain with $W_{nj} = w_n^N(x_j,s_n)$ and $\Phi_{nj} = \phi_n^N(x_j,s_n)$. The solution to our problem, involves the following steps.

- **Step 1:** Define, $\hat{\chi}_\mathbf{n} = \begin{bmatrix}\hat{\mathbf{W}}_\mathbf{n} & | & \hat{\Phi}_n\end{bmatrix}^T$
- **Step 2:** Define the matrices, $\mathbf{KA}, \mathbf{KI}, \mathbf{MA}, \mathbf{MG}, \mathbf{MI}, \mathbf{P}$ and $\mathbf{L}$ as,

  $$KA_{ij} = GK\int_0^L A(x)N'_{v_w i}N'_{w j}dx, \quad KI_{ij} = E\int_0^L I(x)N'_{v_\phi i}N'_{\phi j}dx,$$

  $$MA_{ij} = \rho\int_0^L A(x)N_{v_w i}N_{w j}dx, \quad MG_{ij} = GK\int_0^L A(x)N_{v_\phi i}N_{\phi j}dx,$$

  $$MI_{ij} = \rho\int_0^L I(x)N_{v_\phi i}N_{\phi j}dx, \quad P_{ij} = GK\int_0^L A(x)N'_{v_w i}N_{\phi j}dx,$$

  $$L_{ij} = GK\int_0^L A(x)N_{v_\phi i}N_{w j}dx,$$

  where, $(.)_{ij}$ and $(.)_{ij}$ are respectively the components of the corresponding matrices $\mathbf{KA}, \mathbf{KI}, \mathbf{MA}, \mathbf{MG}, \mathbf{MI}, \mathbf{P}$and $\mathbf{L}$.
- **Step 3:** Define $\mathbf{K_D} = \begin{bmatrix}\mathbf{KA}+\mathbf{MA} & -\mathbf{P} \\ -\mathbf{L} & \mathbf{KI}+\mathbf{GA}+\mathbf{MI}\end{bmatrix}$. Thus Eq. 39) and (Eq. 40) can be represented in matrix form as, $\mathbf{K_D}\begin{bmatrix}\hat{\mathbf{W}}_\mathbf{n} & | & \hat{\Phi}_n\end{bmatrix}^T = \begin{bmatrix}\hat{\mathbf{V}} & | & \hat{\mathbf{M}}\end{bmatrix}^T$.

- **Step 4:** Solve for $\hat{\chi}_{\mathbf{n}}$, such that $[K_D]\hat{\chi}_{\mathbf{n}} = \hat{\mathbf{F}}_{\mathbf{v}}$ is satisfied. where, $\hat{\chi}_{\mathbf{n}}$, which is the vector containing nodal variables at all the nodal points of $\hat{w}_n$ and $\hat{\phi}_n$, is the solution in the frequency domain and $\hat{\mathbf{F}}_{\mathbf{v}}$ is the vector with the shear force and the moment force appended.
- **Step 5:** Extract $\hat{\mathbf{W}}_{\mathbf{n}}$ and $\hat{\Phi}_n$ from $\hat{\chi}_{\mathbf{n}}$. Convert $\hat{\mathbf{W}}_{\mathbf{n}}$ and $\hat{\Phi}_n$ into time domain using inverse Laplace Transform.

6.2 Collocation approach

The collocation approach for the cantilever beam with uniform cross-section is derived in detail in [Vinita, Gopalakrishnan, and Mani (2013)]. In this section we discuss only the collocation approach for the Timoshenko for varying cross-section. The collocation approach for the uniform cross-section can be derived directly from the varying case, by taking $A(x) = A_0$ and $\frac{dA(x)}{dx} = 0$, throughout the length of the beam.

The method of obtaining the solution using collocation approach is different from the other approaches. In collocation approach, the solution to the weighted integral form of the wave equation for the Timoshenko beam (Eq. 37) and (Eq. 38) in frequency domain is obtained by considering the test functions, $v(x)$, $v_w(x)$ and $v_\phi(x)$ respectively for each equation as a Dirac Delta distribution. Hence, $v_{(.)_i}(x) = \delta(x - x_i)$, and the trial function, ϕ_i is taken either as Chebyshev or Legendre polynomials and the residual is made to be zero at the collocation points. The solution is obtained as follows:

We need to solve for $\hat{\mathbf{W}}_{\mathbf{n}}$ and $\hat{\Phi}_n$ in frequency domain as solution to the weak form for $n = 0, 1, 2, ..., N_s - 1$ given by,

$$\int_0^L GK(A(x)(N_w'(x)\hat{\mathbf{W}}_{\mathbf{n}}))'\delta(x-x_i)dx - \int_0^L GK(A(x)(N_\phi(x)\hat{\Phi}_n))'\delta(x-x_i)dx$$
$$- \int_0^L s_n^2 \rho A(x)(N_u(x)\hat{\mathbf{W}}_{\mathbf{n}})\delta(x-x_i)dx = 0 \tag{41}$$

$$\int_0^L E(I(x)(N_\phi'(x)\hat{\Phi}_n))'\delta(x-x_i)dx + \int_0^L GK(A(x)(N_w'(x)\hat{\mathbf{W}}_{\mathbf{n}}))\delta(x-x_i)dx$$
$$- \int_0^L GK(A(x)(N_\phi(x)\hat{\Phi}_n))\delta(x-x_i)dx - \int_0^L s_n^2 \rho I(x)(N_\phi(x)\hat{\Phi}_n)\delta(x-x_i)dx = 0 \tag{42}$$

The weak form defined by (Eq. 41) and (Eq. 42), now reduces to the strong form

of the solution defined at the collocation points $0 < x_i < L$, i.e.,

$$GKA(x_i)N_w''(x_i)\hat{\mathbf{W}}_\mathbf{n} + GKA'(x_i)N_w'(x_i)\hat{\mathbf{W}}_\mathbf{n} - GKA(x_i)N_\phi'(x_i)\hat{\Phi}_n \ldots \\ \ldots - GKA'(x_i)N_\phi(x_i)\hat{\Phi}_n - s_n^2\rho A(x_i)N_w(x_i)\hat{\mathbf{W}}_\mathbf{n} = 0 \tag{43}$$

$$EI(x_i)N_\phi''(x_i)\hat{\Phi}_n + EIA'(x_i)N_\phi'(x_i)\hat{\Phi}_n + GKA(x_i)N_w'(x_i)\hat{\mathbf{W}}_\mathbf{n} \ldots \\ \ldots - GKA(x)N_\phi(x_i)\hat{\Phi}_n - s_n^2\rho I(x_i)N_\phi(x_i)\hat{\Phi}_n = 0 \tag{44}$$

The important point here is that the equation satisfies for all x_i only in $(0,L)$, except at the boundary. Hence, we have to impose the boundary conditions:

At $x_i = 0$ as, $\quad \sum_{j=0}^{N} N_{wj}(x_0)\hat{W}_{nj} = 0$, $\sum_{j=0}^{N} N_{\phi\,j}(x_0)\hat{\Phi}_{nj} = 0$ and

At $x_i = L$ as, $\quad GK\sum_{j=0}^{N} A(x_N)N_{wj}'(x_N)\hat{W}_{nj} = \hat{V}_L$ or $E\sum_{j=0}^{N} I(x_N)N_{\phi\,j}'(x_N)\hat{\Phi}_{nj} = \hat{M}_L$

The residuals of the differential (Eq. 17) and (Eq. 18) for varying cross-section in frequency domain are given as,

$$R_w(x,s_n)_\Omega = GK\frac{d}{dx}\left(A(x)\left(\frac{d}{dx}\hat{w}_n^N(x,s_n) - \hat{\phi}(x,s_n)\right)\right) - s_n^2\rho A(x)\hat{w}_n^N(x,s_n), \\ R_\phi(x,s_n)_\Omega = E\left(I(x)\frac{d}{dx}\hat{\phi}(x,s_n)\right) + GKA(x)\left(\frac{d}{dx}\hat{w}_n^N(x,s_n) - \hat{\phi}(x,s_n)\right)\ldots \\ -s_n^2\rho I(x)\hat{\phi}_n^N(x,s_n), \text{for} \quad 0 < x < L \tag{45}$$

$$R_{w0}(x,s_n)_{\partial\Omega} = \hat{w}_n^N(0,s_n) - w(0,s_n), \quad R_{\phi 0}(x,s_n)_{\partial\Omega} = \hat{\phi}_n^N(0,s_n) - \phi(0,s_n) \tag{46}$$

$$R_{wL}(x,s_n)_{\partial\Omega} = GA(L)\left(\frac{d\hat{w}_n^N}{dx}(L,s_n) - \hat{\phi}(x,s_n)\right) - \hat{V}_L \quad \text{or,}$$

$$R_{\phi L}(x,s_n)_{\partial\Omega} = EI(L)\frac{d\hat{\phi}_n^N}{dx}(L,s_n) - \hat{V}_L \tag{47}$$

Comparing the residual in $0 < x < L$ given by (Eq. 45) with equation (Eq. 43) and (Eq. 44) we see that $R(x_i,s_n)_\Omega = 0$. Similarly comparing the residuals at the boundary $x_i = 0$ given by (Eq. 46), and for the residual at $x_i = L$ given by (Eq. 47) with the corresponding boundary conditions at $x_i = 0$, and $x_i = L$, we see that $R_{w0}(0,s_n)_{\partial\Omega} = 0$ and $R_{\phi 0}(0,s_n)_{\partial\Omega} = 0$ for $x_i = 0$ and $R_{wL}(L,s_n)_{\partial\Omega} = 0$ and $R_{\phi L}(L,s_n)_{\partial\Omega} = 0$ for $x_i = L$.

Thus, the residual is forced to be zero at the collocation points, leading to $(N+1)$ algebraic equations. The two set of $(N+1)$ algebraic equations are solved to obtain $\hat{\mathbf{W}}_\mathbf{n}$ and $\hat{\Phi}_n$. We convert $\hat{\mathbf{W}}_\mathbf{n}$ and $\hat{\Phi}_n$ into time domain using inverse Laplace transform. The advantage of collocation approach, is that the integration process

involved in obtaining all the matrices $[KA],[KI],[MA],[MG],[MI],[P]$ and $[L]$ is avoided. This results in a drastic reduction of computation time. But, it is difficult to form a generalised stiffness matrix as the boundary conditions are to be imposed for a general solution.

7 Results and Discussion

In this section, we present the numerical results obtained for all the four problems (Problems (i) to (iv)) obtained using different numerical methods such as Galerkin, Petrov-Galerkin, Method of Moments and the Pseudo-spectral method. The numerical results obtained is first compared with the problems for which exact solution is available (Problem (i) to (iii)). For Problem (i) and (ii), we discuss the effect of the number of FFT points (N_s), the number of segments (S) and the order of the polynomial (N) used for approximation. We then show the numerical results of Problem (ii) for different values of taper parameter m and it is then compared with the exact solution.

We have considered a Gaussian pulse for Problem (i) and Problem (ii). But for the Timoshenko beam we consider the modulated pulse. The FFT magnitudes with frequency for both the Gaussian and the modulated pulse is shown in (Fig. 5). The group velocities for the different modes such as the shear mode and the bending mode for Problem (iii) are also shown in (Fig. 5). For a modulated pulse, we are able to separate the shear mode and the bending mode as is clear from (Fig. 5). But in the case of a Gaussian pulse, since cut-off frequency for the Timoshenko beam of uniform cross-section (Problem (iii)) is at $f_{c0} = \frac{1}{2\pi}\sqrt{\frac{GA_0K}{\rho I_0}}$, and hence the shear mode will not be visible.

The numerical solution to Problem (iii) is also sought and compared with the exact solution available. We also separate the shear mode and the bending mode numerically for Problem (iii). The group speeds for Problems (i) to (iii) can be computed exactly. The group speed for Problem (i) and (ii) are constant and is independent of frequency, but for Problem (iii) and (iv), the group speeds vary with frequency. Also, the group speeds for Problem (iv) is not available analytically. Hence, we first determine numerically the group speeds for Problem (iii) for which the group speeds can be computed exactly. We then compare the numerical results with the exact results. Finally, for Problem (iv), we also plot the group speed with frequency by observing the group speeds numerically for the shear mode and bending mode for varying frequencies. We also observe that the group speeds vary with the taper parameter m. An approximate expression for calculating the cut-off frequency and the group speeds corresponding to the shear mode and the bending mode is also obtained.

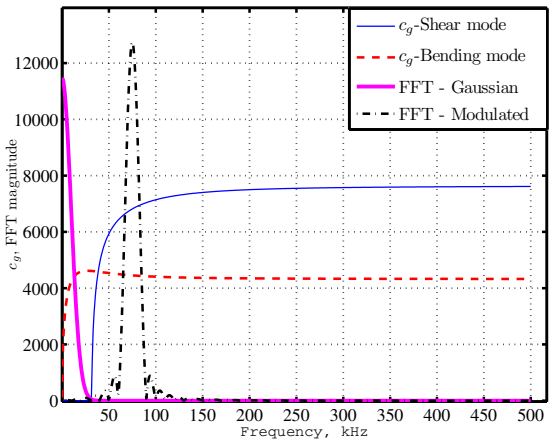

Figure 5: Effect of the Gaussian pulse and the Modulated pulse

7.1 Advantages of frequency domain analysis over time domain analysis

A comparitive study of the frequency domain (both Fourier transform and Laplace Transform method) and the time domain analysis for Problem (i) in detailed in [Vinita, Gopalakrishnan, and Mani (2013)]. In the report we have used the Newmark integration scheme for time marching for Problem (i).

The time domain approximation of the solution and frequency domain approximation with the Galerkin method considering Chebyshev polynomial as the trial function was studied in detail in [Vinita, Gopalakrishnan, and Mani (2013)]. In frequency domain approach, for the number of FFT points $N_s = 256$, with $T = 1$ *milli* secs and $\Delta t = \frac{T}{N_s} = 3.9\mu$ secs, the error was of the order of 10^{-5}, whereas for time domain approach the number of discretisation points required N_t was 1000, with $\Delta t = 1\mu$ secs. It is also interesting to note that for computation in frequency domain, we need to compute only upto $\frac{N_s}{2} = 128$, which even reduces the computational time. As Δt, was increased to 3μ secs, it was observed that the algorithm becomes unstable.

A comparison of the mean squarred error (MSE) and maximum error (Err_{max}) for time and frequency domain methods are shown in (Tab. 1). We have considered the number of FFT points, N_s and the number of time discretisation points, N_t as 1024, ($N_s = N_t$). In time domain analysis, we require $\Delta t < \Delta t_{critical}$, where $\Delta t_{critical} = \frac{\Omega_{crit}}{\omega_{max}}$. Hence, we have chosen a higher value for N_s and have taken $N_s = N_t$ for

comparison. The parameters for the time stepping algorithm, $\gamma = \frac{1}{2}$ and $\beta = 0$. The details of the parameters are given in [Vinita, Gopalakrishnan, and Mani (2013)]. In (Tab. 1), we fix the number of degrees of freedom N_g, in the spatial domain as 55 and vary the number the order of polynomial (N) per segment and the number of segments (S), such that $N_g = SN + 1 = 55$.

From the table we see that the sampling time Δt has to be decreased for the time domain analysis as we increase the order of the polynomial (N), so that $\Delta t < \Delta t_{critical}$ [Vinita, Gopalakrishnan, and Mani (2013)]. This is because the resonant frequencies ω depends upon stiffness and mass matrix $[K]$ and $[M]$ respectively. Also, sampling time, Δt is correspondingly decreased by increasing N_t. Also, increase in N_t increase the computational time drastically. In the case of time domain analysis, when we increase the number of nodes per segment to 19, we require $N_t = 3000$ with $\Delta t = 0.33\ \mu$ seconds. For the same case in the frequency domain analysis, we need to compute the solution $\hat{u}_n(x, \omega_n)$, only upto $\frac{N_s}{2} = 512$, which considerably reduces the computational time in frequency domain approach. The effect of the sampling time Δt, with variation in the design parameter γ is also studied in our report [Vinita, Gopalakrishnan, and Mani (2013)].

However, the frequency domain approach using Discrete Fourier Transform leads to wrap around effects, which can be avoided either by increasing the time window, or by using a throw off element, by taking a Laplace transform or Wavelet transforms of the unknown function. In the case of the Laplace transform the damping factor is selected using the Wilcox and Wedepohl methods [Murthy, Gopalakrishnan, and Nair (2011)], which needs to be designed.

7.2 Effect of the selection of grid points

For Collocation approach, the MSE and Err_{max} for CGL (Chebyshev Gauss Lobotto), LGL (Legendre Gauss Lobotto) and equidistant points are shown in (Tab. 2). The Legendre polynomials were chosen as the trial function (ϕ_i). We see from Table (2) that CGL points have the least error. Thus, for all our analysis, CGL points were considered for the above reason. The details are studied in [Vinita, Gopalakrishnan, and Mani (2013)].

7.3 Effect of various parameters on the solution of the Cantilever beam and Timoshenko beam

It is of interest to study the effect of the number of FFT points (N_s), number of segments (S), the order of the polynomial (N) required for approximation, the effect of taper parameter m and the effect of frequency f, for various numerical methods on the solution of the Cantilever beam and the Timoshenko beam.

Table 1: Error Analysis for Galerkin Method in Time Domain and Frequency Domain

Galerkin Approach		Frequency Domain			Time Domain		
No. of Nodes/Seg. (N+1)	No of Seg. S	$N_s, \Delta t$	MSE	Err_{max}	$N_t, \Delta t$	MSE	Err_{max}
3	27		9.28E-6	2.09E-6	$N_t = 1024, \Delta t = 0.98\ \mu$ secs	1.66E-5	3.51E-6
4	18		1.07E-6	2.40E-7	$N_t = 1024, \Delta t = 0.98\ \mu$ secs	2.36E-5	5.05E-6
					$N_t = 1428, \Delta t = 0.70\ \mu$ secs	1.23E-5	2.02E-6
7	9	$N_s = 1024, \Delta t = 0.98\ \mu$ secs	1.35E-8	2.47E-9	$N_t = 1024, \Delta t = 0.98\ \mu$ secs	2.42E-5	5.15E-6
10	6		8.05E-10	1.35E-10	$N_t = 1428, \Delta t = 0.70\ \mu$ secs	1.29E-5	2.16E-6
19	3		9.23E-12	1.14E-12	$N_t = 3000, \Delta t = 0.33\ \mu$ secs	5.00E-6	6.24E-7
28	2		1.20E-12	1.50E-13	$N_t = 4000, \Delta t = 0.25\ \mu$ secs	4.93E-6	6.53E-7
55	1		1.52E-12	2.55E-13	$N_t = 8000, \Delta t = 0.125\ \mu$ secs	2.55E-6	2.33E-7

Table 2: Error Analysis for Collocation method considering different grid points

Grid points	No. of Nodes/ Segment	No. of Segments	CGL points		LGL points		Equidistant points	
			MSE	Err_{max}	MSE	Err_{max}	MSE	Err_{max}
N_g	$N+1$	S						
16	16	1	1.46E-4	1.64E-5	1.31E-1	3.06E-2	2.85E+0	5.85E-1
31		2	2.53E-6	2.43E-7	6.28E-6	7.25E-7	2.87E-2	7.60E-3
46		3	4.29E-8	6.70E-9	1.57E-7	2.47E-8	4.45E-5	1.70E-5
61		4	1.61E-9	2.71E-10	5.78E-9	9.90E-10	7.95E-7	1.29E-7
76		5	9.06E-11	1.56E-11	3.20E-10	5.50E-11	4.34E-8	8.08E-9
91		6	6.02E-12	1.19E-12	2.11E-11	4.22E-12	2.94E-10	5.97E-10

7.3.1 Effect of N_s (Number of FFT points)

The results for different FFT points for Problem (i) and (ii) for the Galerkin and Collocation method are compared with the exact solution and is shown in (Fig. 6) and (Fig. 7) respectively. In our approach we have considered the following: $N_s = 128, 256, 512$ and 1024, $N = 4$, $S = 12$, $N_g = SN + 1 = 49$, taper parameters for Problem (ii) - $m = 1$ and $a = 0.5$, trial function - Chebyshev. In order to increase the time window, sampling time is taken as $\Delta t = 3\ \mu$ seconds. It is observed that even for $N_s = 128$, the wrap around effect is avoided.

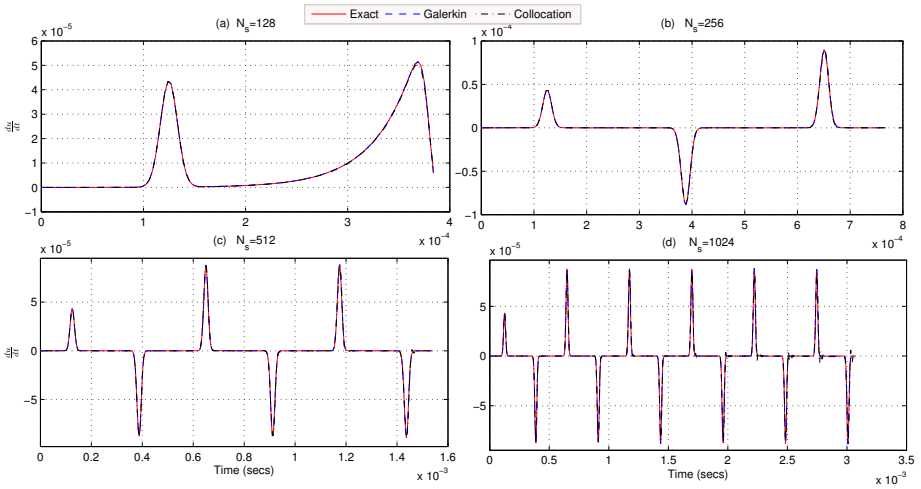

Figure 6: Problem (i): Effect of N_s for different FFT points (128, 256, 512 and 1024) with $dt = 3\mu$ secs

For Problem (iii), we consider the following: $N_s = 512$ and 1024, $N = 30$, $S = 8$, $N_g = SN + 1 = 121$, Length of the finite beam $L = 2$ m, trial function - Legendre. In order to keep the time window constant, sampling time is $\Delta t = 2$ and 1 μ seconds. The variation of the transverse velocity with time for different FFT points is plotted for Galerkin approach, and Collocation approach for Problem (iii) as shown in (Fig. 8). We obtained similar results for the Petrov-Galerkin and Method of Moments approach, and hence not shown here.

7.3.2 Effect of S (Number of segments)

In the finite element analysis, the beam element length, L is divided into finite element or segments S. An N^{th} order polynomial approximation is used per segment.

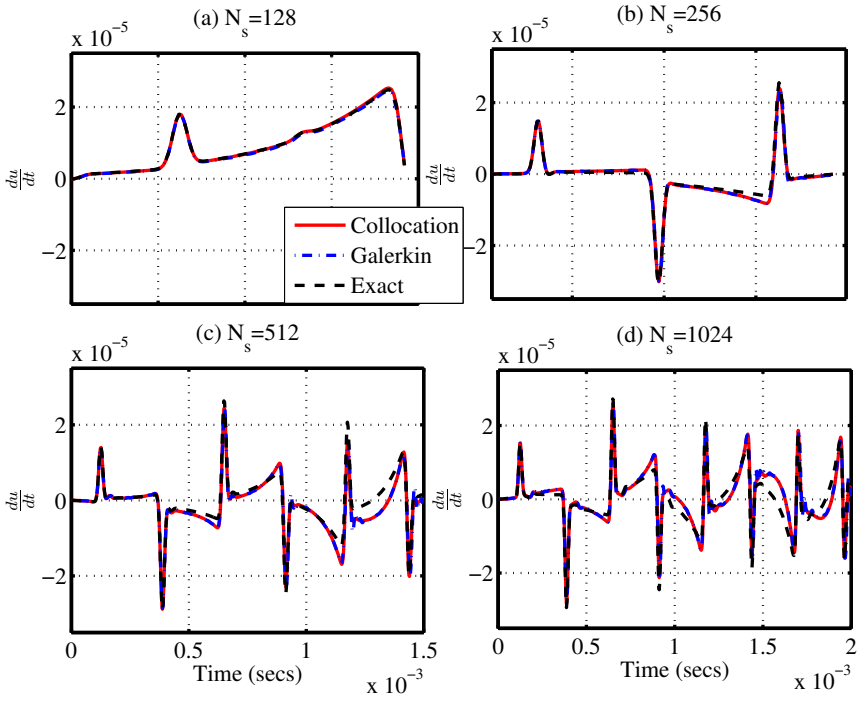

Figure 7: Problem (ii): Effect of N_s for different FFT points (128, 256, 512 and 1024) with $dt = 3\mu$ secs

Thus, each segment will have $N+1$ nodes. For a fixed degree of freedom (DOF), N_g, the number of segments (S) and the number nodes per segment ($N+1$) are selected such that $SN+1 = N_g$. This helps in selecting a polynomial of lower order. In order, to study the effect of the number of segments (S), we kept the order of polynomial (N) fixed in each segment and varied the number of segments S. Here, we have considered the following parameters for Problem (i) and (ii): $N_s = 512$, $\Delta t = 1$ μ seconds, order of the polynomial per segment, $N = 2$, with number of nodes per segment, $(N+1 = 3)$, $S = 8, 16, 32, 64$ with $N_g = SN+1 = 17, 33, 65, 129$. Taper parameters for Problem (ii) - $m = 1$ and $a = 0.5$, Trial function - Chebyshev. The variation of velocity with time is plotted for Galerkin and Collocation approach for Problem (i) and (ii) as shown in (Fig. 9) and (Fig. 10) respectively. The results are compared with the exact solution. Here, it is seen from this figure that in frequency domain analysis, the approximate solution approaches the exact solution as we increase the number of segments, when the order of the polynomial is low.

For Problem (iii), we have considered the following parameters: $N_s = 1024$, $\Delta t = 1\ \mu$ seconds, order of the polynomial per segment, $N = 30$, with number of nodes per segment, $(N+1=3)$, $S = 3,5$, $N_g = SN+1 = 91,151$, Trial function -

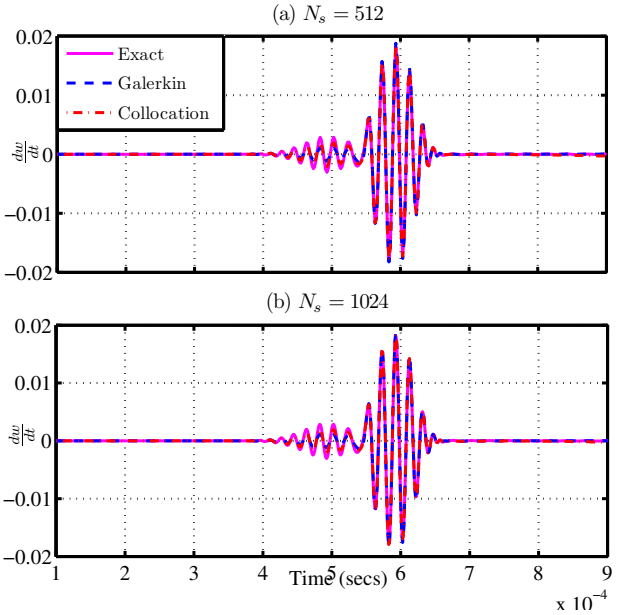

Figure 8: Problem (iii): Effect of N_s for different FFT points (512 and 1024) with $dt = 2$ and 1μ secs

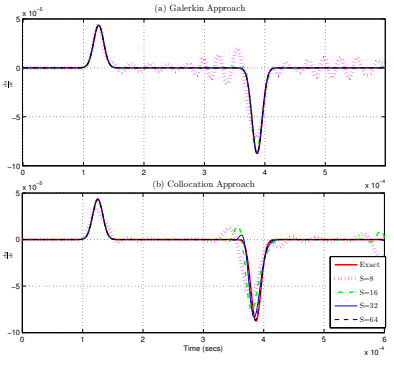

Figure 9: Problem (i): Effect of S for $N = 3$

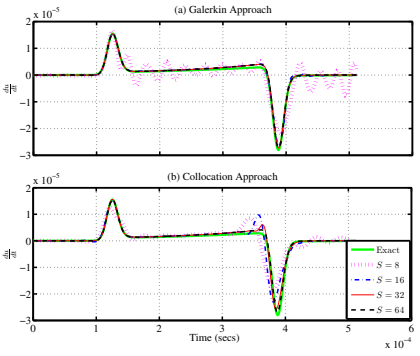

Figure 10: Problem (ii): Effect of S for $N = 3$

Chebyshev. The variation of transverse velocity with time is plotted for Galerkin and Collocation approach for Problem (iii) as shown in (Fig. 11) and (Fig. 12) respectively. The results are compared with the exact solution. Here, it is seen from this figure that in frequency domain analysis, the approximate solution approaches the exact solution as we increase the number of segments, when the order of the polynomial is low.

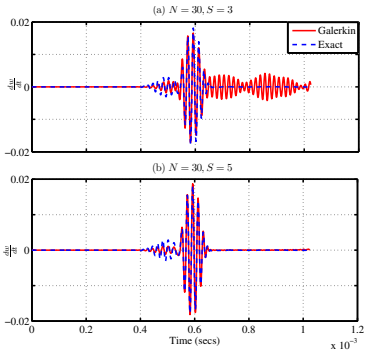

Figure 11: Problem (iii): Effect of S for $N = 30$ for Galerkin approach

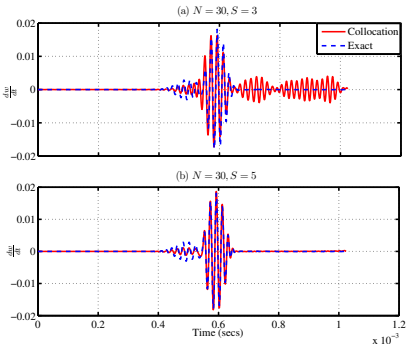

Figure 12: Problem (iii): Effect of S for $N = 30$ for Collocation approach

7.3.3 Effect of N (order of the polynomial)

To study the effect of the order of the polynomial (N), in each segment, we fix number of segments and vary the number of nodes per segment. For Problem (i) and (ii), we have considered the following parameters: $N_s = 512$, $\Delta t = 1$ μ seconds, order of the polynomial per segment, $N = 2, 6, 9, 11$, with number of nodes per segment, $(N+1 = 3, 7, 10, 12)$, $S = 8$, $N_g = SN + 1 = 17, 49, 57, 89$, taper parameters for Problem (ii) - $m = 1$ and $a = 0.5$, Trial function - Chebyshev. The variation of velocity with time is plotted for Galerkin and Collocation approach for Problem (i) and (ii) as shown in (Fig. 13) and (Fig. 14) respectively. The results are compared with the exact solution.

We have given a detailed study of the error analysis of the different numerical methods for Problem (i) in [Vinita, Gopalakrishnan, and Mani (2013)]. To study the effect of the order of the polynomials (N), we considered the Collocation approach. The variation of mean squared error (MSE) with N_g is shown in (Fig. 15) and the variation of maximum error (Err_{max}) with N_g is shown in (Fig. 16). The MSE and Err_{max} decreases as we start increasing the number of nodes per segment. As the order of the polynomial (N) increases per segment, the convergence rate also

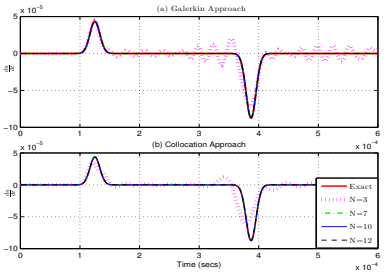

Figure 13: Problem (i): Effect of N for fixed number of segments ($S = 8$)

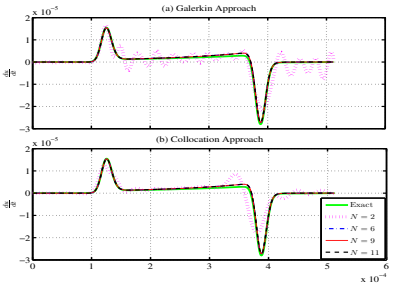

Figure 14: Problem (ii): Effect of N for fixed number segments ($S = 8$)

increases. These figures show an exponential convergence and the exponential decrease in error and is proportional to the order of the polynomials (N). For Problem

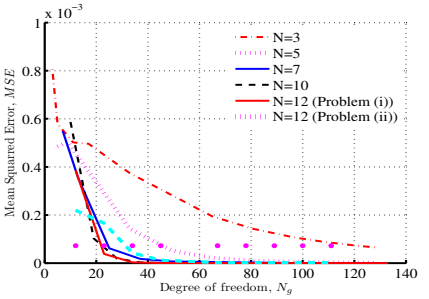

Figure 15: Probem (i): MSE for collocation approach for different order of polynomial

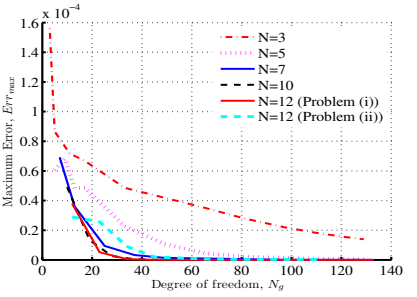

Figure 16: Problem(i): Max. Error for collocation approach for different order of polynomial

(iii), we have considered the following parameters: $N_s = 1024$, $\Delta t = 1$ μ seconds, order of the polynomial per segment, $N = 20, 27$, with number of nodes per segment, $(N+1 = 21, 28)$, $S = 5$, $N_g = SN+1 = 101, 136$, Trial function - Chebyshev. The variation of velocity with time is plotted for Galerkin and Collocation approach for Problem (iii) as shown in (Fig. 17) and (Fig. 18). The results are compared with the exact solution. The (Fig. 9) and (Fig. 13), (Fig. 10) and (Fig. 14), (Fig. 11) and (Fig. 17) and (Fig. 12) and (Fig. 18) show that the approximating polynomial converges to the exact solution with lesser number of segments (S), for higher order of polynomial (N), taken per segment. We obtained similar results for the Petrov-Galerkin and Method of Moments approach, and hence not shown here.

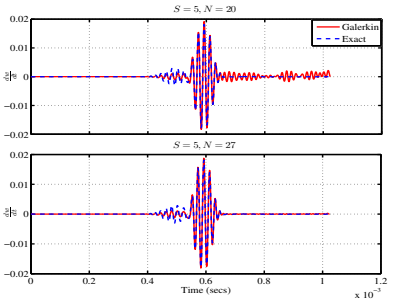

Figure 17: Problem (iii): Effect of N considering fixed number of segments ($S = 5$) for Galerkin approach

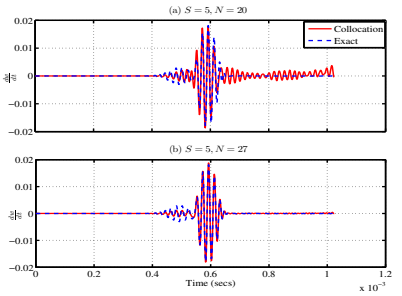

Figure 18: Problem (iii): Effect of N considering fixed number of segments ($S = 5$) for Collocation approach

7.3.4 *Effect of taper parameter m*

The results for Problem (ii) with varying cross-section is compared with the exact solution by considering $a = 1$ and for varying taper parameter $m = 1,2,3,4$. Here we have taken the modulated pulse as the force (F_L) acting at $x = L$. We have considered the following parameters: $N_s = 1024$, $\Delta t = 1\ \mu$ seconds, $N = 9$, $S = 8$, $N_g = SN + 1 = 81$, Trial function - Legendre. The axial velocity for varying m is

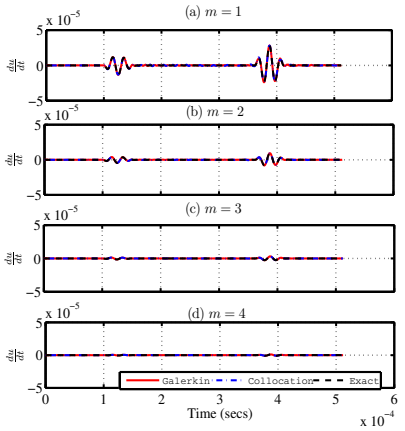

Figure 19: Problem (ii): Comparison with the exact method for varying taper parameter m

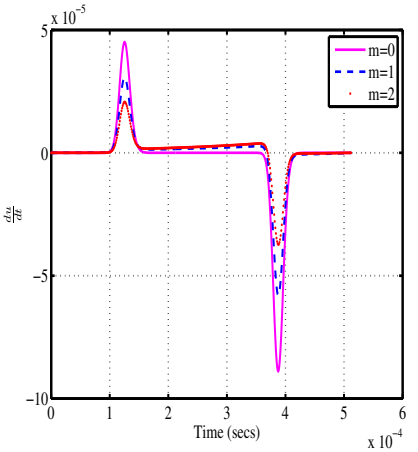

Figure 20: Axial velocity for the cantilever beam with uniform ($m = 0$) and varying cross-section ($m = 1,2$)

shown for the Galerkin and Collocation approach and is compared with the exact solution. Here we require a higher degree of freedom since we have considered the modulated pulse for comparison instead of the Gaussian pulse. From (Eq. 19), we find that as m increases the magnitude of the pulse decreases, but the group velocity remains constant.

We also compare the results of Problem (i) with Problem (ii) in (Fig. 20). It is seen from (Fig. 20) that the group velocity is independent of the taper parameter m and the area of cross-section.

For Problem (iv), we do not have an exact solution and hence we use numerical methods for solution of the tapered Timoshenko beam. We also compare the solution by splitting up the beam into S stepped segments of uniform cross-section and form the exact solution for each segment. We then obtain the Laplace spectral finite element solution (LSEM). The numerical methods such as Galerkin, Petrov-Galerkin, Method of Moments and the Pseudo-spectral methods are then compared with the approximate spectral finite element solution obtained.

The results of the transverse velocity for taper parameter $m = 1,2,3,4$ for the Galerkin and Pseudo-spectral method with comparison to the LSEM are shown in (Fig. 21) and (Fig. 22) respectively. The corresponding group speeds for each case is also shown in the figures. The figures show that the group speeds vary with the taper parameter m. The approximate results using LSEM and the numerical methods are found to be very close to each other.

7.3.5 Effect of f (Frequency of the input pulse)

The effect of frequency of the modulated pulse on the shear and the bending modes are shown in (Fig. 23). We see that the shear mode disappears for low frequencies for Problem (iii) with constant area of cross-section A_0. The shear mode is seen to be prominent for high frequency input pulse of 75 kHz (Fig. 23-(c)).

7.4 Group speeds, c_g

In this section we consider, the group speeds of the cantilever beam and the Timoshenko beam. The group speeds can be computed exactly for Problem (i), (ii) and (iii). For Problem (iv), we use the numerical methods for computation of the group speeds and show that the group speeds vary with taper parameter m.

7.4.1 Problem (i) and (ii): Cantilever beam

The group speeds for Problem (i) and Problem (ii) is a constant and is given by $\sqrt{\frac{E}{\rho}}$. Thus the group speeds are independent of the frequency and taper parameter m.

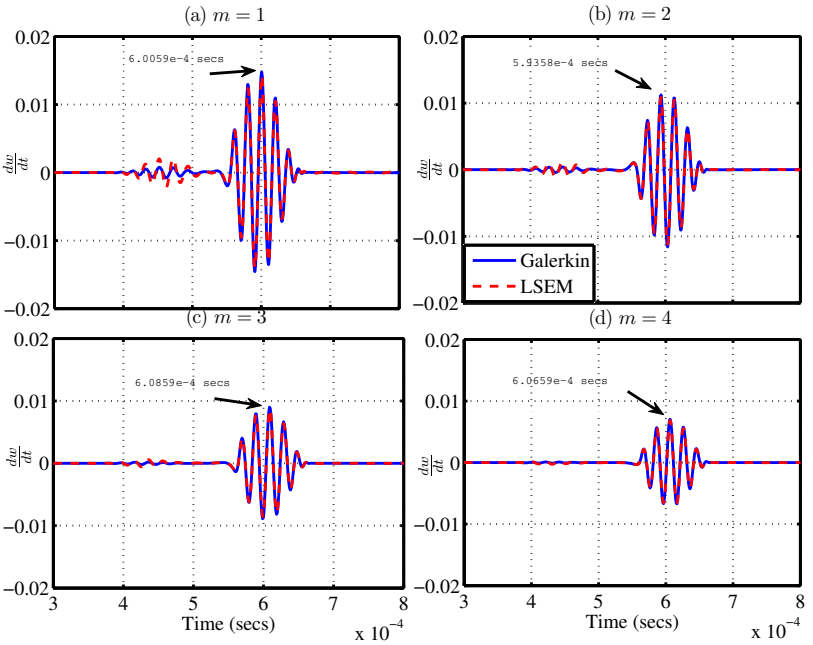

Figure 21: Problem (iv): Effect of taper parameter m on the shear modes and bending modes - Galerkin Method

7.4.2 Problem (iii): Timoshenko beam of uniform cross-section

The group speed of the Timoshenko beam with uniform cross-section computed exactly is plotted in (Fig. 24). The group speeds for the shear mode and the bending mode are shown separately in (Fig. 24.(a)) and (Fig. 24.(b)) respectively. It is seen that the group speeds vary with frequency for the Timoshenko beam, whereas the group speed is a constant for the Cantilever beam. The group speeds for Problem (iii) are also observed numerically, by varying the frequency f of the input pulse. The corresponding velocities are tabulated and the data is interpolated to obtain the group speeds at different frequencies. The group speeds obtained numerically is also shown in (Fig. 24). We see that the group speed obtained numerically is very close to the exact group speeds computed from (Eq. 32).

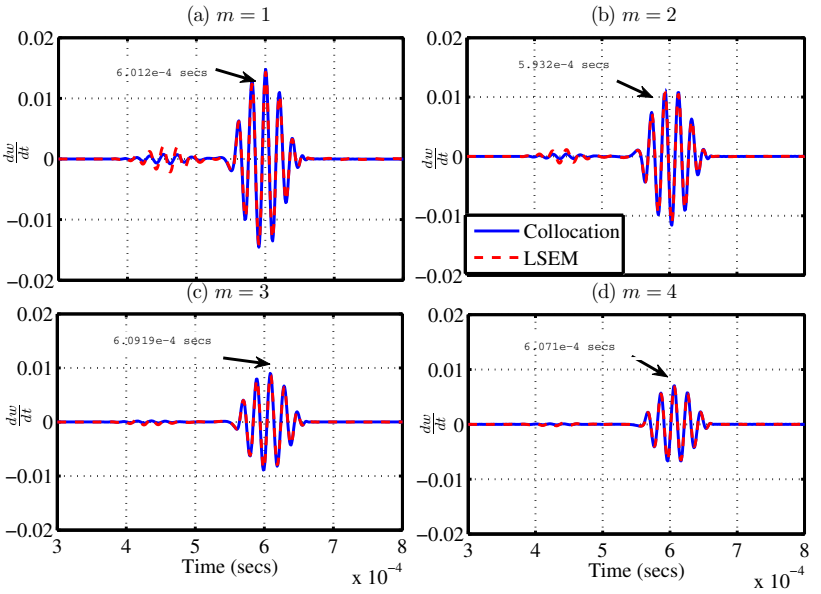

Figure 22: Problem (iv): Effect of taper parameter m on the shear modes and bending modes - Pseudo-spectral Method

7.4.3 Problem (iv): Timoshenko beam of varying cross-section

The group speeds for varying cross-section cannot be computed exactly for the Timoshenko beam. Hence the corresponding group speeds for varying parameter $m = 1,2,3$ and 4 are computed numerically, by varying the frequency of the input pulse. From the transverse velocity graph, we get the corresponding time taken for the shear mode and the bending mode to occur. The corresponding group velocities for each case ($m = 1,2,3,4$) is then tabulated and the data can be interpolated to get the group speeds for different frequencies. This is shown in (Fig. 25).

Now consider the group speed, $c_{g_{ni}}$ for the Timoshenko beam of uniform cross-section for the shear mode and the bending mode as given by (Eq. 32). For Problem (iv), the different modes are a function of x, as they vary with the area of cross-section $A(x)$ and the moment of inertia $I(x)$, along the length of the beam as,

$$k_{bn}(x) = \sqrt{\frac{\rho I(x)}{EI(x)}}s_n, \quad k_{sn}(x) = \sqrt{\frac{\rho A(x)}{GA(x)K}}s_n, \quad k_{cn}(x) = \sqrt{\frac{\rho A(x)}{EI(x)}}s_n \tag{48}$$

For our analysis we consider the LSEM, where we divide the whole length into a

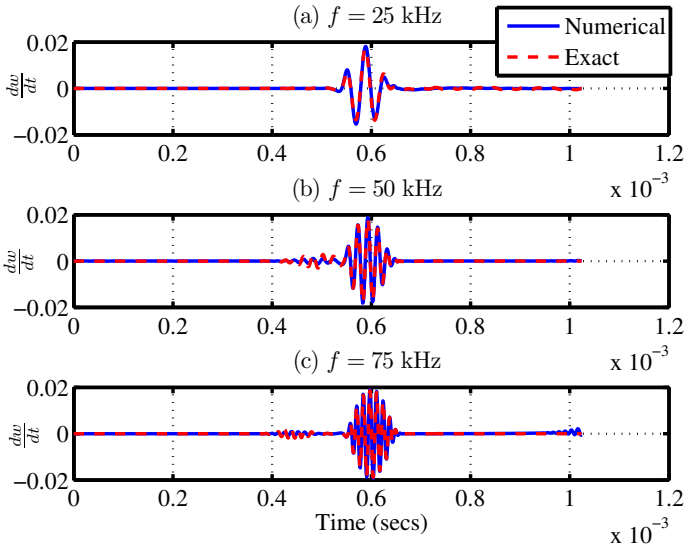

Figure 23: Problem (iii): Effect of the frequency f of the input pulse on the shear mode and the bending modes

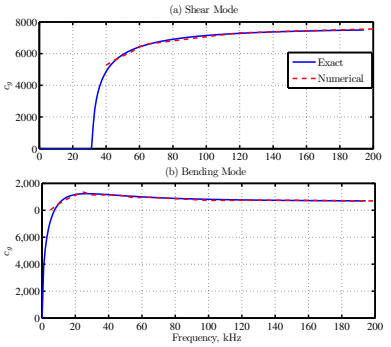

Figure 24: Problem (iii): Group speeds of Timoshenko beam with uniform cross-section

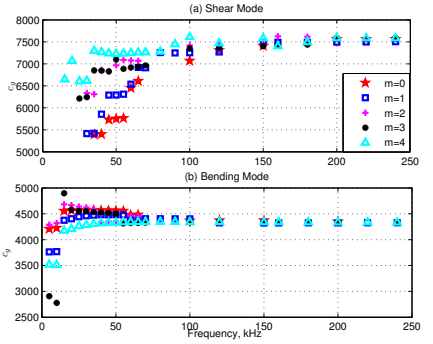

Figure 25: Problem (iv): Group speeds of Timoshenko beam with varying cross-section

number of segments of uniform length. Thus, we get a band of group speeds for each m as shown in (Fig. 26). We observe that the boundaries of the band match the

values of $m = 0$ and $m = 4$, with the numerical results obtained using the Galerkin, Petrov-Galerkin, Method of Moments and Pseudo-spectral approach and is shown in (Fig. 26). Hence, we can approximate the group speeds of the varying case (Problem (iv)) by (Eq. 49) as,

$$c_{g_{ni}} \approx \lim_{x \to L} \frac{2k_{ni}(x)}{-(k_b(x)^2 + k_s(x)^2)\omega_n \pm \frac{2(k_b(x)^2 - k_s(x)^2)\omega_n^3 - 4k_c(x)^2\omega_n}{2\sqrt{(k_{bn}(x)^2 - k_{sn}(x)^2) - 4k_c n(x)^2}}} \tag{49}$$

$$\text{where } k_b(x) = \sqrt{\frac{\rho I(x)}{EI(x)}}, \quad k_s(x) = \sqrt{\frac{\rho A(x)}{GA(x)K}}, \quad k_c(x) = \sqrt{\frac{\rho A(x)}{EI(x)}} \tag{50}$$

The cut off frequency for Problem (iv) can also be approximated as,

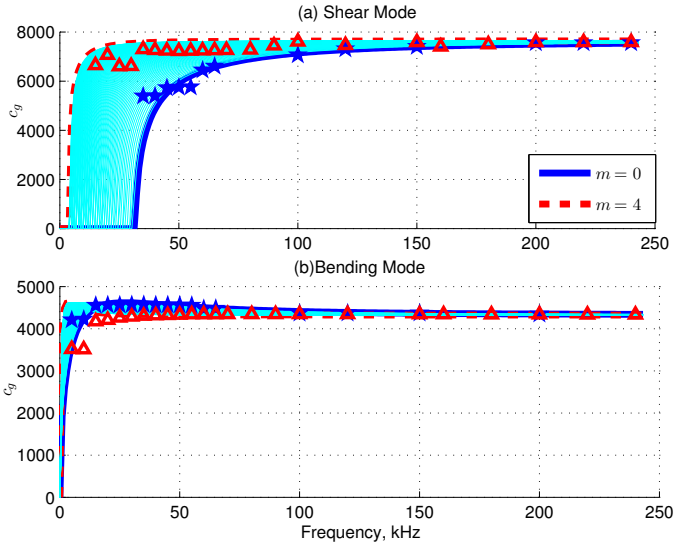

Figure 26: Problem (iv): Group speeds of Timoshenko beam with varying cross-section using approximate expression

$$f_c \approx \frac{1}{2\pi}\sqrt{\frac{GKA(x)}{\rho I(x)}} = \frac{1}{2\pi}\sqrt{\frac{GKA_0}{\rho I_0}}\sqrt{\frac{1}{(1+\frac{\varepsilon x}{L})^{2m}}} = \frac{1}{(1+\frac{\varepsilon x}{L})^m}\, f_{c0} \tag{51}$$

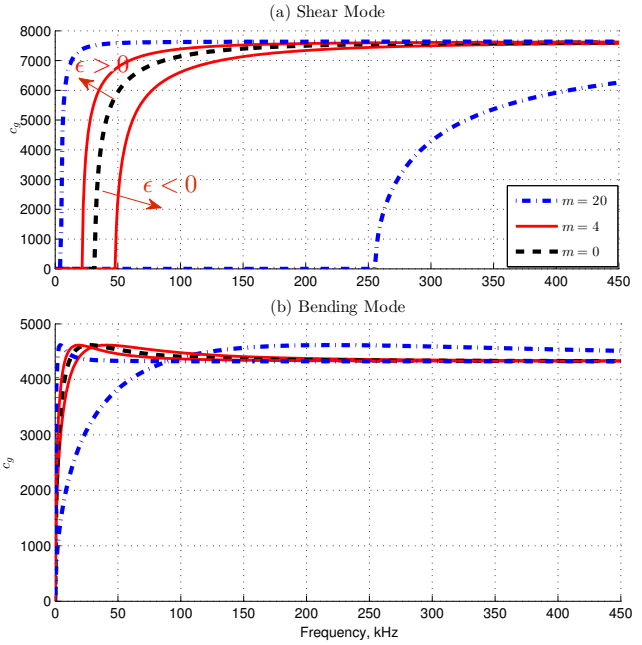

Figure 27: Problem (iv): Group speeds of Timoshenko beam showing variation in cutoff frequency with m and ε

where f_{c0} is the cut off frequency for the Timoshenko beam of uniform cross-sectional area A_0. Hence we can say that,

$$\lim_{m\to\infty} f_c \approx \lim_{m\to\infty} \frac{1}{(1+\frac{\varepsilon x}{L})^m} f_{c0} = 0, \quad \text{for } \varepsilon > 0 \tag{52}$$

$$\lim_{m\to\infty} f_c \approx \lim_{m\to\infty} \frac{1}{(1+\frac{\varepsilon x}{L})^m} f_{c0} = \infty, \quad \text{for } \varepsilon > 0$$

(Fig. 27) shows the approximate group speeds for $\varepsilon = 0.1$ and $\varepsilon = -0.1$ for $m = 0, 4, 20$. (Fig. 27) also shows that the cut-off frequency decreases as m increases for $\varepsilon > 0$, and the cut-off frequency increases as m increases for $\varepsilon < 0$.

8 Conclusion

The Cantilever beam with uniform and varying area of cross-section (Problem (i) and (ii)) and the Timoshenko beam with uniform and varying area of cross-section

(Problem (iii) and (iv)) are solved in the frequency domain using different numerical methods such as the Galerkin approach, Petrov-Galerkin approach, Method of Moments approach and the Pseudo-spectral approach. We have compared all the numerical methods with the exact solution available for Problem (i), and (iii). For the Cantilever problem with varying coefficient (Problem (ii)), exact solutions are not available for all the cases. We have considered a special case for which exact solution is available in the form of Bessel functions and have compared the numerical results for varying taper parameter m. Laplace spectral methods are used to solve the problem exactly in frequency domain for Problem (i), (ii) and (iii). An infinite element (throw-off element) at both the ends for Problem (iii) is formulated for avoiding reflections from the boundary. This allows two formulations for the Timoshenko beam namely the Fourier transform approach and the Laplace transform approach.

The approximation of the integral for calculating the stiffness matrix and mass matrix for the Galerkin, Petrov-Galerkin and Method of Moments approach is done using GLL integration. For the Pseudo-spectral or Collocation approach the integration is not required and hence reduces the computational time. A numerical solution is obtained for Problem (iv) using all the numerical methods discussed above and also using Laplace spectral element method.

The numerical solution for the set of ODEs in frequency domain for the Cantilever beam and the Timoshenko beam is obtained using variational principles and the results are presented.

(1) The effect of the number of FFT points (N_s) used for frequency domain method is studied for Problem (i), (ii) and (iii). It is observed that the frequency domain analysis gives results very close to the exact solution even for $N_s = 256$.

(2) The effect of the order of the polynomial N per segment used for the approximation of the unknown function is studied for Problem (i), (ii) and (iii). The MSE and Err_{max} is low as the order of the polynomial increases for the same degree of freedom. The higher order of polynomial also reduces the error of integral approximation.

(3) The effect of number of segments S used is also studied for Problem (i), (ii) and (iii). It is shown that for a lower order polynomial approximation, the numerical solution approaches the exact solution as we increase the number of segments.

(4) The effect of the frequency of the input pulse on the group speeds for the Cantilever beam (Problem (i) and (ii)) and the Timoshenko beam (Problem (iii) and

(iv)) are also studied. It is shown that the group speeds are a constant for the Cantilever beam and the group speed vary with frequency for the Timoshenko beam.

(5) It is also shown that a modulated pulse is able to extract the shear mode and the bending mode of the Timoshenko beam (Problem (iii) and (iv)).

(6) We show that the effect of taper parameter m does not affect the group speed for Problem (ii), whereas it is shown numerically that the group speeds vary correspondingly for the shear mode and bending mode for Problem (iv). The group speeds are obtained numerically by varying the frequency of the input pulse and are tabulated for varying frequency for different taper parameter m.

(7) An approximate expression for the group speeds and the cut off frequency and it is compared with the results obtained numerically. We also show that the cut-off frequency disappears for large m for $\varepsilon > 0$ and increases for large m for $\varepsilon < 0$.

The numerical methods in frequency domain are able to obtain the same results as the exact solution for Problem (i), Problem (ii) and Problem (iii). Hence, we obtain the shear mode and bending mode for the Timoshenko beam with varying cross-section (Problem (iv)) using all the numerical methods. The group speeds are also obtained numerically for the Timoshenko beam with varying cross-section for varying frequency and varying taper parameter m.

References

Atluri, S. N.; Cho, J. Y.; Kim, H. G. (1999): Analysis of thin beams, using the meshless local petrov galerkin method, with generalized moving least squares interpolations. *Computational Mechanics, Springer-Verlag*, vol. 24, pp. 334–347.

Atluri, S. N.; Shen, S. (2005): Simulation of a 4th order ode: Illustration of various primal & mixed mlpg methods. *CMES*, vol. 7, no. 3, pp. 241–268.

Black, K. (1995): A petrov-galerkin spectral element technique for heterogeneous porous media flow. *Journal of Computers and Mathematics with Applications*, vol. 29, no. 1, pp. 49–65.

Boyd, J. P. (2000): *Chebyshev and Fourier Spectral Methods*. Dover Publications, Inc., NewYork.

Canuto, C.; Quarteroni, A.; Hussaini, M. Y.; Zang, T. A. (2006): *Spectral Methods: Fundamentals in Single Domains*. Springer, NewYork.

Chakraborty, A.; Gopalakrishnan, S. (2003): A spectrally formulated finite element for wave propagation analysis in functionally graded beams. *International Journal of Solids and Structures*, vol. 40, pp. 2421–2448.

Cohen, G. C. (2002): *Higher-Order Numerical Methods for Transient Wave Equations*. Springer, NewYork.

Doyle, J. F. (1999): *Wave Propagation in Structures*. Springer, NewYork.

Doyle, J. F.; Farris, T. N. (1990): A spectrally formulated finite element for flexural wave propagation in beams. *International Journal of Analytical and Experimental Modal Analysis*, vol. 5, pp. 13–23.

Doyle, J. F.; Farris, T. N. (1990): A spectrally formulated finite element for wave propagation in 3-d frame structures. *International Journal of Analytical and Experimental Modal Analysis*, pp. 223–237.

Godinho, L.; Soares Jr., D. (2012): Frequency domain analysis of fluid-solid interaction problems by means of iteratively coupled meshless approaches. *CMES*, vol. 2248, no. 1, pp. 1–28.

Godinho, L.; Soares Jr., D. (2013): Frequency domain analysis of interacting acoustic-elastodynamic models taking into account optimized iterative coupling of different numerical methods. *Journal of Engineering Analysis with Boundary Elements*, , no. 37, pp. 1074–1088.

Gopalakrishnan, S.; Chakraborty, A.; Mahapatra, D. R. (2006): *Spectral Finite Element Method: Wave Propagation, Diagnostics and Control in Anisotropic and Inhomogeneous Structures*. Springer, NewYork.

Gopalakrishnan, S.; Martin, M.; Doyle, J. F. (1992): A matrix methodology for spectral analysis of wave propagation in multiple connected timoshenko beam. *Journal of Sound and Vibration*, vol. 158, pp. 11–24.

Iura, M.; Suetake, Y.; Atluri, S. N. (2003): Accuracy of co-rotational formulation for 3-d timoshenko beam. *CMES*, vol. 4, no. 2, pp. 249–258.

Khater, A. H.; Temsah, R. S. (2008): Numerical solutions of the generalized kuramoto sivashinsky equation by chebyshev spectral collocation methods. *Journal of Computers and Mathematics with Applications*, pp. 1465–1472.

Lathi, B. P. (1998): *Signal Processing and Linear Systems*. Berkeley-Cambridge Press, CA.

Long, S.; Atluri, S. N. (2002): A meshless local petrov-galerkin method for solving the bending problem of a thin plate. *CMES*, vol. 3, no. 1, pp. 53–63.

Mahapatra, D. R.; Gopalakrishnan, S. (2003): A spectral finite element model for analysis of axial flexural shear coupled wave propagation in laminated composite beams. *Composite Structures*, pp. 67–88.

Mitra, M.; Gopalakrishnan, S. (2006): Wavelet based spectral finite element modelling and detection of de-lamination in composite beams. In *Proceeding of the Royal Society A*, pp. 1721–1740.

Murthy, M. V. V. S.; Gopalakrishnan, S.; Nair, P. (2011): Signal wrap-around free spectral finite element formulation for multiple connected finite 1-d waveguides. *Journal of Aerospace Sciences and Technologies*, vol. 63, no. 1, pp. 72–88.

Reddy, J. N. (2005): *An Introduction to the Finite Element Method*. 3rd ed., McGraw-Hill Education.

Salehi, R.; Dehghan, M. (2012): The use of a legendre pseudospectral viscosity technique to solve a class of nonlinear dynamic hamilton jacobi equations. *Journal of Computers and Mathematics with Applications*, pp. 629–644.

Saravi, M.; Babolian, E.; England, R.; Bromilow, M. (2008): System of linear ordinary differential and differential-algebraic equations and pseudo-spectral method. *Journal of Computers and Mathematics with Applications*, pp. 1524–1531.

Vinita, C.; Gopalakrishnan, S.; Mani, V. (2013): Frequency and time domain solution of 1-d wave equation: An exhaustive study of issues, challenges and performance analysis. Technical Report AE-CG-VM-SG-2013, Indian Institute of Science, Bangalore, India, 2013.